Bounding generalization error with input compression: An empirical study with infinite-width networks

Anonymous authors
Paper under double-blind review

Abstract

Estimating the Generalization Error (GE) of Deep Neural Networks (DNNs) is an important task that often relies on availability of held-out data. The ability to better predict GE based on a single training set may yield overarching DNN design principles to reduce a reliance on trial-and-error, along with other performance assessment advantages. In search of a quantity relevant to GE, we investigate the Mutual Information (MI) between the input and final layer representations, using the infinite-width DNN limit to bound MI. An existing input compression-based GE bound is used to link MI and GE. To the best of our knowledge, this represents the first empirical study of this bound. In our attempt to empirically stress test the theoretical bound, we find that it is often tight for best-performing models. Furthermore, it detects randomization of training labels in many cases, reflects test-time perturbation robustness, and works well given only few training samples. These results are promising given that input compression is broadly applicable where MI can be estimated with confidence.

1 Introduction

Generalization Error (GE) is the central quantity for the performance assessment of Deep Neural Networks (DNNs), which we operationalize as the difference between the train-set accuracy and the test-set accuracy[1]. Bounding a DNN's GE based on a training set is a longstanding goal (Jiang et al., 2021) for various reasons: i) Labeled data is often scarce, making it at times impractical to set aside a representative test set. ii) The ability to predict generalization is expected to yield overarching design principles that may be used for Neural Architecture Search (NAS), reducing a reliance on trial-and-error. iii) Bounding the error rate is helpful for model comparison and essential for establishing performance guarantees for safety-critical applications. In contrast, the test accuracy is merely a single performance estimate based on an arbitrary and finite set of examples. Furthermore, the *adversarial examples* phenomenon has revealed the striking inability of DNNs to generalize in the presence of human-imperceptible perturbations (Szegedy et al., 2014; Biggio & Roli, 2018), highlighting the need for a more specific measure of *robust* generalization.

Various proxies for DNN complexity which are assumed to be relevant to GE—such as network depth, width, ℓ_p-norm bounds (Neyshabur et al., 2015), or number of parameters—do not consistently predict generalization in practice (Zhang et al., 2021). In search of an effective measure to capture the GE across a range of tasks, we investigate the Mutual Information (MI) between the input and final layer representations, evaluated solely on the training set. In particular, we empirically study the Input Compression Bound (ICB) introduced by (Tishby, 2017; Shwartz-Ziv et al., 2019), linking MI and several GE metrics. An emphasis on *input* is an important distinction from many previously proposed GE bounds (e.g., Zhou et al. (2019)), which tend to be *model*-centric rather than *data*-centric.

We use *infinite ensembles of infinite-width networks* (Lee et al., 2019), as the MI quantity we examine is ill-defined in deterministic DNNs (Goldfeld et al., 2019). Infinite-width networks correspond to *kernel regression* and are simpler to analyze than finite-width DNNs, yet they exhibit double-descent and overfitting phenomena observed in deep learning (Belkin et al., 2019). For these reasons, Belkin et al. (2018) suggested that understanding kernel learning should be the first step taken towards understanding generalization in

[1]GE is also referred to as *generalization gap*. Note that some use "generalization error" as a synonym for "test error".

deep learning. To this end, we evaluate the ICB proposed by Tishby (2017); Shwartz-Ziv et al. (2019) with respect to three axes of performance:

1. First, we verify whether the bound holds in practice by evaluating the GE of a variety of models, composed by drawing random metaparameters of the neural architecture and training procedure. We then compare the empirical GE to the theoretical GE bound given by ICB. We show that ICB contains the GE at the expected 95% confidence level for three of five datasets, or all five for the best-performing models. In addition, we suggest the training-label randomization test (Zhang et al., 2017) as a means to determine when ICB may perform well a priori without relying on a test set.

2. Next, we analyze whether the ICB is sufficiently small for useful model comparisons. If a theoretical GE bound exceeds 100% in practice, it is said to be *vacuous*. As we study binary classification tasks we additionally require that the bound be less than 50% for models with non-trivial GE. We show that ICB is often sufficiently close to the empirical GE, and thus presents a *non-vacuous* bound, obtained from less than 2000 training samples.

3. Last, we assess the *correlation* between ICB and GE. Ranking GE is less consistent when several metaparameters vary, with ICB sometimes outperforming, and at times under-performing a simpler baseline. Increasing the Neural Tangent Kernel (NTK) diagonal regularization coefficient is most correlated with reducing ICB.

Beyond these three main desiderata for generalization bounds, we show advantages in reducing ICB even when the GE is small. Reducing ICB on *natural* training labels prevents models from fitting *random* labels, and conversely, ICB *increases* when models are trained on *random* versus *natural* training labels (Zhang et al., 2017; 2021). Finally, we show that ICB is predictive of test-time perturbation robustness (Goodfellow et al., 2015; Gilmer et al., 2019), without assuming access to a differentiable model.

2 Background

We make use of an information-theoretically motivated generalization bound, the ICB, to establish an overlooked link between MI and GE. The bound seems to have first appeared in a lecture series (see, e.g., Tishby (2017)), later in a pre-print (Shwartz-Ziv et al., 2019)[Thm. 1] and more recently in a thesis (Shwartz-Ziv, 2022)[Ch. 3]. To the best of our knowledge the bound has not yet been studied empirically.

2.1 Mutual information in infinite-width networks

The MI between two random variables X and Z is defined as

$$I(X;Z) \equiv \sum_{x,z} p(x,z) \log \frac{p(x,z)}{p(x)p(z)} = \mathbb{E}_{p(x,z)} \left[\log \frac{p(z|x)}{p(z)} \right], \tag{1}$$

where we used Bayes' rule to obtain the expression on the right and introduced $\mathbb{E}_{p(x,z)}[\cdot]$ to denote the average over $p(x,z)$. In our case, X denotes the input, and Z the input representation which is taken as the Neural Network (NN) output. Since the marginal $p(z)$ is unknown, we use an unnormalized multi-sample "noise contrastive estimation" (InfoNCE) variational bound. The InfoNCE procedure was originally proposed for unsupervised representation learning (van den Oord et al., 2018), which also serves as a lower bound on MI (Poole et al., 2019). In van den Oord et al. (2018), the density ratio $p(z|x)/p(z)$ was learned by a NN. Instead, following Shwartz-Ziv & Alemi (2020), we use infinite ensembles of infinitely-wide NN, which have a conditional Gaussian predictive distribution: $p(z|x) \sim \mathcal{N}\left(\mu(x,\tau), \Sigma(x,\tau)\right)$ with μ, Σ given by the NTK and Neural Network Gaussian Process (NNGP) kernel (Jacot et al., 2018). The predictive distribution also remains Gaussian following τ steps of Gradient Descent (GD) on the Mean-Squared Error (MSE) loss. The conditional Gaussian structure given by NTK may be supplied in the InfoNCE procedure, yielding MI bounds free from variational parameters. Specifically, we use the "leave one out" upper bound (Poole et al., 2019)

on MI to conservatively bound MI:

$$I(X;Z) \leq \mathbb{E}\left[\frac{1}{N}\sum_{i=1}^{N}\log\frac{p(z_i|x_i)}{\frac{1}{N-1}\sum_{j\neq i}p(z_i|x_j)}\right] = I_{\mathrm{UB}}. \tag{2}$$

A lower bound on MI, I_{LB}, of a similar form as equation 2 is also available (equation 5, Appendix A.2), and we verified that both bounds yield similar results for the training regime in which we apply them (Fig. A5). See van den Oord et al. (2018) and Poole et al. (2019) for formal derivations of equation 2 and equation 5. These MI bounds must be computed on the training set only to evaluate a *generalization* bound.

2.2 Input compression bound

Here, we provide an intuitive explanation of the ICB building on existing results and using information theory fundamentals (Cover & Thomas, 1991). A more formal derivation including a proof can be found in Shwartz-Ziv et al. (2019)[Appendix A]. We begin with the conventional GE bound developed in the Probably Approximately Correct (PAC) framework, which plays a central role in the early mathematical descriptions of machine learning. It is assumed that a model receives a sequence of examples x, each labeled with the value $f(x)$ of a particular target function, and has to select a hypothesis that approximates f well from a certain class of possible functions. By relating the hypothesis-class cardinality $|\mathcal{H}|$, the confidence parameter δ, and the number of training examples N_{trn}, one obtains the following bound on the GE:

$$\mathrm{GE} < \sqrt{\frac{\log(|\mathcal{H}|) + \log(1/\delta)}{2N_{\mathrm{trn}}}}\,. \tag{3}$$

The key term in this bound is the hypothesis-class cardinality, the *expressive power* of the chosen ansatz. For a finite $\mathcal{H}$, it is simply the number of possible functions in this class; when $\mathcal{H}$ is infinite, a discretization procedure is applied in order to obtain a finite set of functions. For NNs, $|\mathcal{H}|$ is usually assumed to increase with the number of trainable parameters. The bound (3) states that generalization is only possible when the expressivity is outweighed by the size of the training set, in line with the well-known bias-variance trade-off of statistical learning theory. Empirical evidence, however, demonstrates that this trade-off is qualitatively different in deep learning, where generalization tends to improve as the NN size increases even when the size of the training set is held constant.

The key idea behind the ICB is to shift the focus from the hypothesis to the *input space*. For instance, consider binary classification where each of the $|\mathcal{X}|$ inputs belongs to one of two classes. The approach that leads to bound (3) reasons that there are $2^{|\mathcal{X}|}$ possible label assignments, only one of which is true, and hence a hypothesis space with $2^{|\mathcal{X}|}$ Boolean functions is required to guarantee that the correct labeling can be learned. The implicit assumptions made here are that all inputs are fully distinct and that all possible label assignments are equiprobable. These assumptions do not hold true in general, since classification fundamentally *relies* on similarity between inputs. However, the notion of similarity is data-specific and a priori unknown; thus, the uniformity assumption is required when deriving a general statement.

The approach behind ICB circumvents these difficulties altogether by applying information theory to the process of NN learning. First, note that solving a classification task involves finding a suitable partition of the input space by class membership. DNNs perform classification by creating a representation Z for each input X and progressively coarsening it towards the class label, which is commonly represented as an indicator vector. The coarsening procedure is an inherent property of the NN function, which is implicitly contained in Z. By construction, the NN implements a partitioning of the input space, which is adjusted in the course of training to reflect the true class membership. In this sense, the cardinality of the hypothesis space reduces to $|\mathcal{H}| \approx 2^{|\mathcal{T}|}$, where $|\mathcal{T}|$ is the number of class-homogeneous clusters that the NN distinguishes. To estimate $|\mathcal{T}|$, the notion of *typicality* is employed: *Typical* inputs have a Shannon entropy $H(X)$ that is roughly equal to the average entropy of the source distribution and consequently a probability close to $2^{-H(X)}$. Since the typical set has a probability of nearly 1, we can estimate the size of the input space to be approximately equal to the size of the typical set, namely $2^{H(X)}$. Similarly, the average size of each partition is given by $2^{H(X|Z)}$. An estimate for the number of clusters can then be obtained by $|\mathcal{T}| \approx 2^{H(X)}/2^{H(X|Z)} = 2^{I(X;Z)}$,

yielding a hypothesis class cardinality $|\mathcal{H}| \approx 2^{2^{I(X;Z)}}$. With this, the final expression for the ICB is:

$$\mathrm{GE}_{\mathrm{ICB}} < \sqrt{\frac{2^{I(X;Z)} + \log(1/\delta)}{2N_{\mathrm{trn}}}}\,, \tag{4}$$

where it is assumed that X is a d-dimensional random variable that obeys an ergodic Markov Random Field (MRF) probability distribution, asymptotically in d (common for signal and image data, see e.g., Murphy (2012)[Ch. 19]). Unfortunately, it is impossible to check this assumption directly because it assumes something about the data-generation process, which we can not access from finite samples (e.g. from `CIFAR-10`). We therefore treat ICB as a tool, and empirically test how useful this tool is in practice. We comment on the ergodic MRF assumption in Appendix A.1. We only evaluate ICB when we can obtain a confident estimate of $I(X;Z)$. For this we require a tight sandwich bound on $I(X;Z)$ with $I_{\mathrm{UB}} \approx I_{\mathrm{LB}}$. We discard samples where $I_{\mathrm{UB}}(X;Z) > \log(N_{\mathrm{trn}})$, since $I_{\mathrm{LB}}(X;Z)$ cannot exceed $\log(N_{\mathrm{trn}})$. See Fig. A5 for typical $I_{\mathrm{UB}}, I_{\mathrm{LB}}$ values during training and samples to discard. Note that the units for $I(X;Z)$ in ICB are *bits*.

3 Experiments

Our experiments are structured around three key questions: 1) To what extent do the ICB assumptions hold in practice? Can we find models with GE that exceeds the theoretical bound (§4.1), or with small predicted GE even when trained on random labels where generalization is impossible (§4.2)? 2) Is the ICB close enough to the empirical GE for useful model comparisons (§4.3)? 3) To what extent does ICB correlate with GE evaluated on standard and robust test sets (§4.4)? Here, we describe the two main experimental procedures, Exp. A (§3.1) and Exp. B (§3.2), in which we draw a population of models for comparison of GEs to the theoretical ICB. We focus on binary classification like much of the generalization literature, which also enables us to more efficiently evaluate MI bounds by processing kernel matrices that scale by N_{trn}^2 rather than $(k \times N_{\mathrm{trn}})^2$ for k-classes. Aside from this computational advantage, our methodology extends to the multi-class setting.

3.1 Evaluating generalization throughout training (Experiment A)

We conduct experiments with five standard benchmark datasets: `MNIST` (LeCun & Cortes, 1998), `FashionMNIST` (Xiao et al., 2017), `SVHN` (Netzer et al., 2011), `CIFAR-10` (Krizhevsky, 2009), and `EuroSAT` (Helber et al., 2018; 2019). These datasets are intended to be representative of low to moderate complexity tasks and make it tractable to train thousands of models (Jiang* et al., 2019). Experiments with `EuroSAT` further demonstrate how the method scales to 64-by-64 pixel images. For each of the image datasets, we devise nine binary classification tasks corresponding to labels "i versus $i+1$" for $i \in \{0, \ldots, 8\}$. Note that this sequential class ordering is an arbitrary choice. We use metaparameters that are common to deep learning, with the exception of "diagonal regularization", which is specific to the NTK, $\mathcal{K}$. It is defined as: $\mathcal{K}_{\mathrm{reg}} = \mathcal{K} + \lambda \frac{\mathrm{Tr}(\mathcal{K})}{N_{\mathrm{trn}}} I$, where λ is a coefficient that controls the amount of regularization. This is analogous to ℓ_2 regularization of finite-width DNNs, only we penalize the parameters' distance w.r.t. their initial values instead of w.r.t. the origin (Lee et al., 2020).

We initialize a variety of models by sampling uniformly at random from the following metaparameters: the number of fully-connected layers, $L \sim \mathcal{U}(1,5)$, the diagonal regularization coefficient $\lambda \sim \mathcal{U}\{10^0, 10^{-1}, 10^{-2}, 10^{-3}, 10^{-4}\}$, the activation function $\phi(\cdot) \sim \mathcal{U}\{\texttt{ReLU}(\cdot), \texttt{Erf}(\cdot)\}$, and the number of training samples, $N_{\mathrm{trn}} \sim \mathcal{U}(250, 2000)$. Test sets have a constant size of $N_{\mathrm{tst}} = 2000$. We do not randomly sample a learning rate or mini-batch size, as the infinite-width networks are trained by full-batch GD, for which the training dynamics do not depend on the learning rate once below a critical stable value (Lee et al., 2019). A nominal learning rate of 1.0 was used in all cases and found to be sufficient.[2] We use 100 different random seeds to draw metaparameters for each of the nine tasks, yielding 900 models for each dataset. Each of these 900 models was evaluated at five different time steps throughout training at $t = \{10^2, 10^3, 10^4, 10^5, 10^6\}$ yielding 4500 tuples (ICB, GE) to analyze. The end points $t = 10^2$ and $t = 10^6$ were selected as most of the variation in GE was contained within this range. Training for less than $t = 10^2$ steps typically resulted in a

[2]This was the default setting in `neural_tangents` software library (Novak et al., 2020).

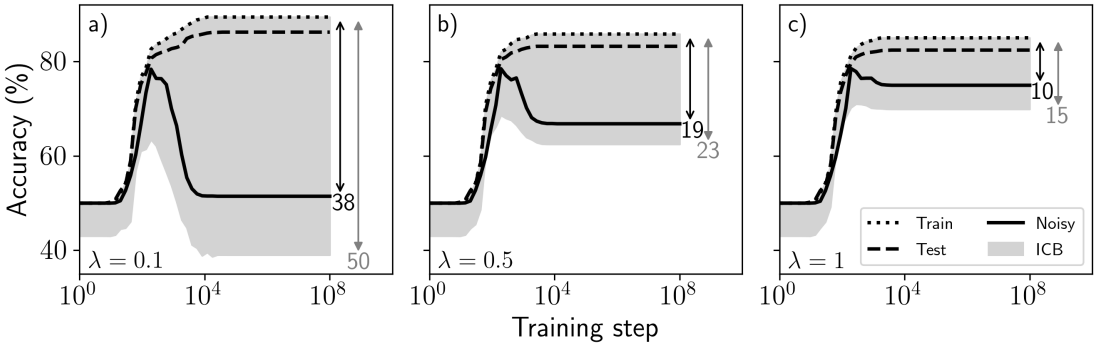

Figure 1: **The ICB may be sensitive to robust GE when it is loose w.r.t. standard GE.** The ICB is plotted as a grey shaded band underneath the training accuracy indicating the range of test accuracy compatible with the theoretical bound. Performance metrics are evaluated for a `EuroSAT Pasture` versus `Sea-Lake` binary classification task using 500 training samples and 2000 test samples and different regularization levels in (a)–(c). At low regularization $\lambda = 0.1$ (a), the ICB is vacuous with respect to standard generalization beyond 10^4 training steps, but reflects the poor robust generalization for the "Noisy" test set with Additive White Gaussian Noise (AWGN). Increasing the regularization to $\lambda = 0.5$ (b) and $\lambda = 1.0$ (c) reduces ICB and the AWGN GE. Arrows indicate the steady-state AWGN GE (black), and ICB (grey) along with their respective values. See Fig. A5 for the corresponding upper and lower $I(X;Z)$ bounds for this experiment.

small GE, as both training and test accuracy were near random chance or increasing in lockstep. In terms of steady-state behaviour, GE was often stable beyond $t = 10^6$. Furthermore, $t = 10^6$ was found to be a critical time beyond which $I_{\mathrm{UB}}(X;Z)$ sometimes exceeded its upper confidence limit of $\log(N_{\mathrm{trn}})$, particularly for small λ values where memorization (lack of compression) is possible.

3.2 Evaluating generalization at steady state (Experiment B)

Binary classification tasks were devised from the same source datasets as in § 3.1. Instead of considering only nine tasks, we enumerated all $\binom{10}{2} = 45$ binary label combinations. For example, for `MNIST`, the classification task of distinguishing digit "0" versus "1", "0" versus "2", and so forth. Here, we used a fixed $N_{\mathrm{trn}} = 1000$ for `MNIST`, `FashionMNIST`, and `EuroSAT`; and $N_{\mathrm{trn}} = 2000$ for `SVHN` and `CIFAR-10`. We perform a uniform random search over: the number of fully-connected layers, $L \sim \mathcal{U}(1,5)$, diagonal regularization coefficient, $\lambda \sim \mathcal{U}(0,2)$, and activation function, $\phi(\cdot) \sim \mathcal{U}\{\texttt{ReLU}(\cdot), \texttt{Erf}(\cdot)\}$. We use 100 different random seeds to draw metaparameters for each of the 45 tasks, yielding 4500 trials for each source dataset. Each of the trials was evaluated at $t = \infty$ yielding 4500 tuples (ICB, GE).

4 Results

Illustrative example Before presenting the main results, we examine ICB for a `EuroSAT` classification task using only 500 training samples (Fig. 1). This is a challenging task, as tight MI and GE bounds are difficult to obtain for high-dimensional DNNs, particularly with few samples. For example, in (Dziugaite & Roy, 2017) 55000 samples were used to obtain a $\approx 20\%$ GE bound for finite-width DNNs evaluated on `MNIST`.

We evaluate ICB throughout training from the first training step ($t = 10^0$) until steady state when all accuracies stabilize ($t = 10^8$). Shortly after model initialization ($t = 10^0$ to $t = 10^1$) the ICB is $< 7\%$ (indicated by the height of the shaded region in Fig. 1) and the training and test accuracy are both at 50% (GE= 0). Here, ICB is non-vacuous, but also not necessarily interesting for this random-guessing phase. ICB increases as training is prolonged.[3] At low regularization (Fig. 1 a), the ICB ultimately becomes vacuous (ICB $\approx 50\%$) around 10^4 steps. However, although ICB is vacuous with respect to *standard* generalization in a), it reflects well the poor *robust* generalization when tested with AWGN (Gilmer et al., 2019). Increasing

[3]It may not be obvious that ICB increases monotonically with training steps as the training accuracy also increases.

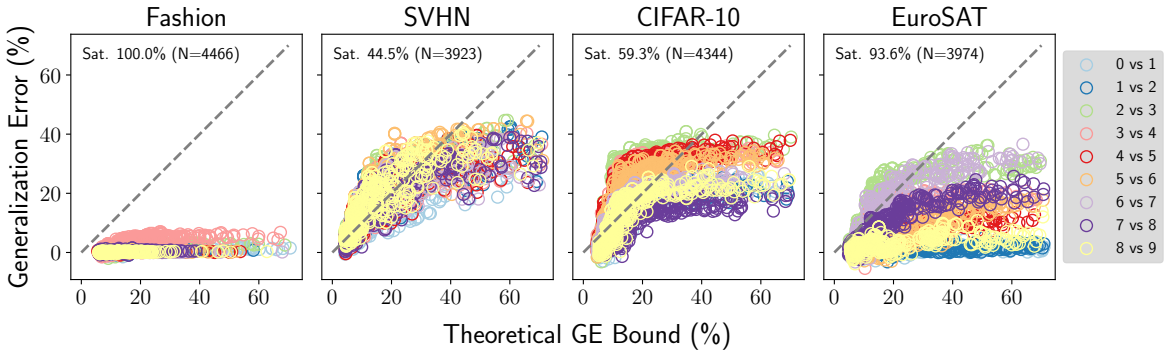

Figure 2: The ICB ("Theoretical GE Bound") is plotted versus GE for `FashionMNIST`, `SVHN`, `CIFAR`, and `EuroSAT` datasets for Exp. A (§3.1). We refer to the percentage of models with GE $<$ ICB as the ICB satisfaction rate, which is annotated in the top left corner of each plot with format "Sat. % (N)", where N denotes the number of valid experiments. Each binary classification task is assigned a unique colour to highlight inter-task differences in ICB satisfaction rate.

Table 1: Overall ICB satisfaction rate (Sat. %) with number of valid experiments N in brackets. Results for Exp. A are also plotted in Figure 2; a more detailed breakdown of these results can be found in Table A6-10.

	`MNIST`	`Fashion`	`SVHN`	`CIFAR`	`EuroSAT`
Exp. A	100% (2237)	100% (4466)	44.5% (3923)	59.3% (4344)	93.6% (3974)
Exp. B	100% (2250)	100% (4500)	27.0% (4500)	68.0% (4500)	95.0% (2221)

the regularization coefficient λ reduces ICB from 50% (a) to 23% (b) and 15% (c), and the robust GE from 38% (a) to 19% (b) and 10% (c).

Both standard and robust GE are bounded at all times by ICB. The latter is, however, a coincidence, as the robust GE is subject to the arbitrary AWGN noise variance ($\sigma^2 = 1/16$). The additive noise variance could be increased to increase the robust GE beyond the range bounded by ICB. More important than bounding the robust GE *absolute percentage* is that ICB captures the trend of robust generalization. Evaluating robustness effectively is error-prone and often assumes access to test data and a differentiable model (Athalye et al., 2018; Carlini et al., 2019). We make no such assumptions here. The lack of robustness in Fig. 1 a) would have likely gone unnoticed. Either early stopping or increasing λ reduce the ICB and robust GE as a potential solution—or a better trade-off between accuracy versus robustness (Tsipras et al., 2019). A caveat to this example is that only two metaparameters varied: the number of training steps t and regularization λ. Next, we assess the ability of ICB to bound and rank GE for a broader range of metaparameters and datasets.

4.1 Bounding generalization error

We refer to the percentage of tuples (ICB, GE) for which GE $<$ ICB as the *"ICB satisfaction rate"*, or *"Sat."* in plots. We expect $\approx 95\%$ of samples to satisfy this property as the bound is evaluated with $\delta = 0.05$ or 95% confidence. The overall ICB satisfaction rate with the respective number of valid experiments N is listed in Table 1. Exp. B yielded greater N than Exp. A primarily because it uses a different range for the regularization coefficient λ, resulting in larger λ values. Since larger λ is associated with more compression, Exp. B had fewer samples being discarded than in Exp. A due to I_{UB} exceeding $\log(N_{\text{trn}})$. Otherwise, ICB satisfaction rates are similar, with `SVHN` performing slightly worse and `CIFAR-10` slightly better for Exp. B versus Exp. A. These results also suggest that exploring nine binary classification tasks (Exp. A) serves as a useful approximation for the full set of all 45 possible tasks (Exp. B). Next, we analyze how model performance influences the ICB satisfaction rate.

When we restrict our scope to the best-performing models based on their test accuracy, the ICB satisfaction rate improves considerably. For example, models with test accuracy $\geq 80\%$ attain ICB satisfaction rates of 94% ($N = 682$) for `SVHN` in Exp. B, and 99% ($N = 2812$) for `EuroSAT` in Exp. A (Fig. A11c). For `CIFAR-10` in Exp. B, we obtain 96% ($N = 591$) by restricting to test accuracy $\geq 87\%$. The specific test accuracy thresholds were chosen to balance a trade-off between satisfying the ICB at $\approx 95\%$ and maximizing N. Although best-performing models are more likely to be deployed in practice, theoretical GE bounds generally prohibit access to a test set. Therefore, we next select models based on their *training* accuracy.

We refer to models that achieve 100% accuracy on the training set as "overfitted", consistent with prior use of this term by Belkin et al. (2018). Interestingly, restricting our analysis to overfitted models either improves or does not change ICB satisfaction rate for Exp. A. For `MNIST`, `FashionMNIST`, `SVHN`, and `EuroSAT`, overfitted models attain an ICB satisfaction rate of 100% with $N = 1970, 1820, 20, 353$ respectively, while for `CIFAR-10`, the satisfaction rate remained below 95%, albeit it improved from 59.3% ($N = 4344$) to 72.6% ($N = 876$). Similar results were observed for Exp. B. (See Figures A7, A8, A9, A10, A11 in the Appendix). The mostly excellent ICB satisfaction rates of the overfitted models are not due to trivially constant GE or ICB values (Figure 3); these models still have considerable variance w.r.t. both metrics despite their identical training accuracies.

Inter-task differences were observed in terms of the ability of ICB to bound GE. For example, for Exp. A, six of nine `EuroSAT` binary classification tasks *always* satisfied ICB ($N = 2534$), whereas two tasks reduced the overall average. The satisfaction rate was only 68% ($N = 468$) for the "2 vs. 3" task and 72% ($N = 475$) for the "6 vs. 7" task (see Fig. A2 and Table A10). These tasks were unusual in that there was a strong inverse relationship between training error and GE, such that reducing the training error resulted in a steady increase in test error, with $\tau \approx -0.9$ for both tasks, compared to $\tau = -0.58$ for the "0 vs. 1" task. The negative correlation between training and test performance for the "2 vs. 3" task also resulted in a lower mean test accuracy ($70.2 \pm 2.2\%$ ($N = 467$)) compared to other tasks, e.g., "0 vs. 1" ($93.5 \pm 5.3\%$ ($N = 415$)), consistent with our previous observation that best-performing models generally satisfy ICB. We further investigated inter-task differences for `EuroSAT` Exp. B, for which all $\binom{10}{2} = 45$ binary classification tasks were evaluated for 50 seeds each. For the two poorly performing tasks "2 vs. 3" and "6 vs. 7", the ICB satisfaction rate was 78% ($N = 50$) and 86% ($N = 50$), respectively. For 34 of 45 tasks ($N = 1913$), ICB was satisfied for all seeds.

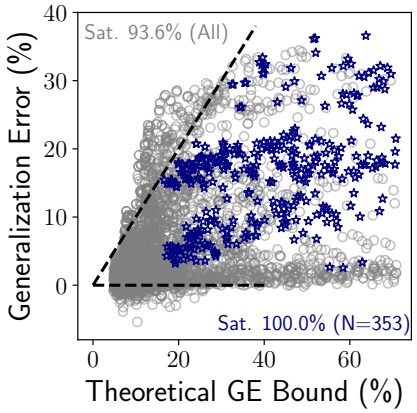

Figure 3: Theoretical GE bound (ICB) versus GE for `EuroSAT` (Exp. A). Overfitted models indicated by stars.

4.2 The randomization test

Zhang et al. (2017; 2021) proposed the "randomization test" after observing that DNNs easily fit random labels. They argue that useful generalization bounds ought to be able to distinguish models trained on *natural* versus *randomized* training labels, since generalization is by construction made impossible in the latter case. However, we cannot necessarily expect a theoretical GE bound to exactly hold for models trained on random labels, since the training and test sets are no longer drawn from the same distribution. We therefore pose the following questions: Q1: *To what extent does the ICB correlate with the ability to fit random labels?* Q2: *Can ICB distinguish training sets with natural versus random labels?* To address Q1, we aim to find metaparameters that reduce ICB and prevent models from fitting *random* training labels, while still permitting them to fit the *natural* training labels. This, however, introduces a potential for confounding if the metaparameter choice alone prevents the model from fitting random labels rather than ICB. For Q2, we hold all metaparameters constant and observe whether ICB changes for randomized training labels. For simplicity, we consider a two-layer fully-connected ReLU network. We train the model to $t = \infty$ on the natural training set ($N_{\text{trn}} = 1000$) with 20 different regularization values λ in the range 10^{-4} to 10^{1}. We measure Kendall's τ ranking between the ICB evaluated on these models and their training accuracies

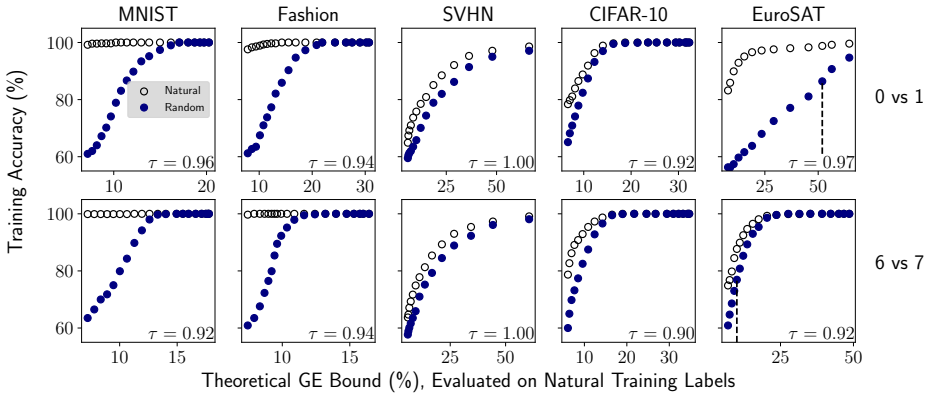

Figure 4: **ICB often distinguishes between natural and randomized training sets.** The accuracy w.r.t. the "Natural" and "Random" training labels is plotted versus the theoretical GE bound (ICB), which is evaluated on the natural training labels. Each data point corresponds to a unique regularization value λ, which influences the ICB value. The top row corresponds to the "0 vs. 1" task and bottom row the "6 vs. 7" task. Considerable separation between natural and random labels for `MNIST`, `FashionMNIST`, and `EuroSAT` is observed. Differences are harder to distinguish for `SVHN` and `CIFAR-10`, but still apparent. ICB is highly correlated with ability to fit random labels in all cases. The broken vertical line for `EuroSAT` indicates the ICB value for which there is at least a 10% accuracy difference between natural versus random sets.

when re-trained with random labels. We find that the ICB value obtained after training on *natural* labels is strongly correlated with the ability to fit *random* labels for all five datasets. Furthermore, competitive accuracy for *natural* training labels is preserved for three of five datasets in doing so (see Fig. 4).

Surprisingly, ICB_{UB} approximates the GE well even when the model is trained on *random labels* (Table 2). For $\lambda = 0.1$, $\text{ICB}_{\text{UB}} = 15.5\%$ compared to a GE of 21.3%. Next, for $\lambda = 0.01$, $\text{ICB}_{\text{UB}} = 38.5\%$ and GE is 39.7%. Last, for $\lambda = 0.001$, $I_{\text{UB}} = 8.96$, which is greater than $\log(N_{\text{train}}) = 6.91$ nats, therefore the corresponding ICB_{UB} of 197.6% should be discarded. In this case, substituting the "optimistic" lower estimate $\text{ICB}_{\text{LB}} = 54.1\% \approx \text{GE} = 50\%$.

Table 2: **ICB increases after training on random labels.** Randomization test results for `EuroSAT`. The lower and upper MI bounds, I_{LB} and I_{UB}, are included for comparison against $\log(N_{\text{trn}}) \approx 6.91$ nats. Columns ICB_{LB} and ICB_{UB} refer to whether I_{LB} or I_{UB} is taken as $I(X;Z)$ estimate, respectively. Columns "Train" and "Test" show the respective accuracy in %. ICB values are larger for random labels when comparing rows with "Train"= 100.0.

λ	I_{LB}	I_{UB}	ICB_{LB}	ICB_{UB}	Train	Test	GE
Natural Training Labels							
10^{-1}	4.87	5.37	26.0	33.1	97.9	98.7	-0.8
10^{-2}	5.40	6.58	33.7	60.2	99.5	98.6	0.9
10^{-3}	5.78	7.40	40.5	90.4	100.0	97.5	2.5
Random Training Labels							
10^{-1}	3.68	3.75	15.0	15.5	71.3	50.0	21.3
10^{-2}	5.28	5.67	31.7	38.5	89.7	50.0	39.7
10^{-3}	6.37	8.96	54.1	197.6	100.0	50.0	50.0

Intuitively, we expect $I(X;Z)$ to be smaller after training on natural labels, since training on random labels requires memorization of random data, i.e., the opposite of compression. However, note that to isolate the effect of the training label type on ICB, the training accuracy must also be controlled, as higher accuracy generally requires greater complexity and thus larger $I(X;Z)$. This intuition is consistent with our results, as both I_{LB} and I_{UB} increase monotonically with the training accuracy for both training label types (see Table 2).

Training with $\lambda = 0.001$ allows models to perfectly fit both natural and randomized training sets (Table 2 column "Train" = 100%), which presents a suitable setting for evaluating whether ICB is sensitive to whether training labels are natural or random. Indeed, I_{LB} is greater for random labels (6.37 vs. 5.78 nats), resulting in

Table 3: **Ability of ICB to separate natural versus random training labels is a good predictor of ICB satisfaction rate by task.** The row "$\text{ICB}_{\text{rand}}@X\%$" indicates the minimum ICB value for which a $X\%$ accuracy difference between natural and random labels is observed. The "Sat. (%)" column showing the ICB satisfaction rate is taken from §4.1, Exp. A. The column τ indicates the rank correlation between $\text{ICB}_{\text{rand}}@X\%$ and Sat. (%) over the nine tasks. Columns sorted by ascending order of $\text{ICB}_{\text{rand}}@X\%$.

EuroSAT	Task	2/3	6/7	3/4	7/8	4/5	5/6	0/1	1/2	8/9	$\tau = 0.76$
	Sat. %	68	72	97	100	100	100	100	100	100	
	$\text{ICB}_{\text{rand}}@10\%$	7.5	10.0	11.2	13.4	19.3	22.5	51.9	59.5	66.9	
CIFAR-10	Task	2/3	5/6	4/5	0/1	3/4	6/7	1/2	8/9	7/8	$\tau = 0.65$
	Sat. %	29	41	39	74	35	68	79	74	97	
	$\text{ICB}_{\text{rand}}@5\%$	6.8	8.1	9.3	9.8	10.4	10.9	11.2	11.3	13.2	

Table 4: **ICB is non-vacuous for best-performing models on five datasets.** The GE (%) of a best-performing model is compared to ICB for each dataset. The column N_{trn} indicates the number of training samples, which was a metaparameter for the first experiment (§3.1, **Exp. A**), and a constant for the second experiment (§3.2, **Exp. B**).

	Exp. A, $t = \{10^2, \ldots, 10^6\}$					**Exp. B**, $t = \infty$				
Dataset	Train	Test	GE	ICB	N_{trn}	Train	Test	GE	ICB	N_{trn}
`MNIST`	100.0	100.0	0.0	11.2	931	99.9	99.9	0.0	12.1	1000
`Fashion`	99.9	100.0	-0.1	7.2	1112	99.9	100.0	-0.1	8.1	1000
`SVHN`	98.8	74.2	24.6	28.0	1564	100.0	90.8	9.3	21.1	2000
`CIFAR`	94.8	89.2	5.6	7.6	1966	99.2	93.8	5.4	11.3	2000
`EuroSAT`	97.8	98.7	-0.9	25.6	1979	100.0	100.0	0.0	22.6	1000

an increase of the *optimistic* theoretical GE bound, ICB_{LB}, from 40.5% to 54.1%. The more *pessimistic* ICB_{UB} increases even more dramatically from 90.4% to 197.6%, which is beyond the valid range of GE ($0 - 100\%$).

The randomization test identifies tasks with low ICB satisfaction rate

Recall from §4.1 that three binary classification tasks were responsible for reducing the ICB satisfaction rate below 100% for `EuroSAT`: "2 vs. 3" (Sat. 68%), "6 vs. 7" (Sat. 72%), and "3 vs. 4" (Sat. 97%) for Exp. A. We observed that these were the *same* tasks for which ICB performed poorly on the randomization test. Specifically, we measured the minimum ICB value for which a 10% or greater percentage difference was detected between the natural and random training-sets (vertical broken line in Fig. 4). The "2 vs. 3" task required the smallest ICB (7.5%) before the difference in label type became apparent. The "6 vs. 7" task had the next highest ICB of 10.0%, followed by "3 vs. 4" with 11.2%. The other six tasks—that have 100% satisfaction rate—have strictly greater ICB (Table 3). Similar results are observed for `CIFAR-10` using a smaller 5% threshold as accuracies for natural and random labels were closer than for `EuroSAT`. The tasks with minimum ("2 vs. 3") and maximum ("7 vs. 8") satisfaction rate are the same tasks with the minimum and maximum $\text{ICB}_{\text{rand}}@5\%$. Therefore, the training-set based randomization test—which only required training a single model here—may be used to help identify when ICB performs well as a GE bound for a variety of models. Our adaptation of the well-known randomization test complements the list of factors already identified in §4.1 as affecting ICB satisfaction rate.

4.3 Vacuous or non-vacuous?

Models with high test accuracy are the more likely to be deployed in practice. To evaluate whether ICB is non-vacuous and close enough to GE to aid model comparison, for each dataset we selected the model with the smallest ICB value among the top-three most accurate models. The ICB values are considerably less than 50% in all cases, satisfying the basic definition of non-vacuous for a binary classification task (Table 4). For Exp. A, the smallest difference between ICB and GE occurred for the `CIFAR` dataset, with a GE of 5.6%

compared to an ICB value of 7.6% for 1966 training samples (Table 4, Exp. A). The greatest ICB value occurred for SVHN (28.0%), however the GE was also large in this case (24.6%).

For Exp. B, both ICB and GE decrease for SVHN (Table 4, Exp. B)) relative to Exp. A. For CIFAR, a similar GE of $\approx 5\%$ is attained as in Exp. A, but with a greater ICB by 3.7%. This may be due to the training accuracy increasing by 4.4% from 94.8% (Exp. A) to 99.2% (Exp. B). In summary, not only is ICB non-vacuous, it is close enough to GE to perform model comparisons.

4.4 Relationship between theoretical bound and generalization error

Here, we evaluate the ability of ICB to rank GEs in terms of Kendall's rank correlation coefficient, τ. Our analysis of correlation between a complexity metric and empirical GE is inspired by previous work (Jiang* et al., 2019; Jiang et al., 2021). Figure A13 helps motivate the use of the ICB for ranking GE rather than using its constituent complexity metric $I(X;Z)$, based on a subset of Exp. B metaparameters. An issue with correlation analysis is that the training-set classification error or proxy loss can serve as a good predictor of GE, therefore Jiang* et al. (2019) train models to a fixed training loss to control for confounding effects. However, fixing the training loss limits the extent of metaparameter exploration. For example, a complexity metric or GE bound may rank GEs of overfitted models well, but perform poorly for early-stopping. To maintain a broad scope, we follow both Exp. A & B procedures and treat the train-set accuracy as a baseline for comparison against ICB, then evaluate overfitted models separately.

Two perturbed test sets help measure correlations between ICB and *robust* GE; as perturbations we use AWGN (Gilmer et al., 2019) and FGSM (Goodfellow et al., 2015). These perturbations are appropriate for evaluating the robustness of infinite-width networks trained by GD, which behave as linear functions of their parameters (Lee et al., 2019). It can be shown that a classifier's error rate for a test set corrupted by AWGN determines the distance to the decision boundary for linear models (Fawzi et al., 2016) and serves as a useful guide for DNNs (Gilmer et al., 2019). For AWGN, we use a Gaussian variance $\sigma^2 = 1/16$ for EuroSAT and $\sigma^2 = 1/4$ for the other datasets. For FGSM, we use a ℓ_∞-norm perturbation of size $4/255$ for inputs $x \in [-1, +1]$.

Table 5: Kendall's τ ranking for three GE types: Clean, AWGN and Fast Gradient-Sign Method (FGSM) for models that obtain zero training error. The number of models is indicated by the N column. NB: The "–" entries for SVHN had $p > 0.05$ when computing τ and were therefore discarded.

Dataset	N	Clean	AWGN	FGSM
MNIST	2329	0.27	0.30	0.29
Fashion	1820	0.39	0.42	0.41
SVHN	20	0.32	–	–
CIFAR	876	0.19	0.20	0.12
EuroSAT	353	0.33	0.38	0.29

In terms of ranking (Clean, AWGN, FGSM) GEs by aggregating all nine tasks for Exp. A, ICB performs better than the training accuracy baseline for MNIST (Table A6) and FashionMNIST (Table A7); slightly worse than the baseline for SVHN (Table A8) and EuroSAT (Table A10); roughly on par with the baseline for CIFAR (Table A8). All overfitted models from the Exp. A procedure have a positive τ-ranking between ICB and the three GE types for all datasets (Table 5). Thus, ICB outperforms the training accuracy baseline ($\tau = 0$) here. For Exp. B, there was considerable variance in τ-rankings among the 45 binary classification tasks for each dataset. Although the median ranking was positive for all datasets, the baseline achieves a higher median ranking than ICB for all three error types (Clean, AWGN, FGSM) (Fig. A12). An ablation study to identify which metaparameters influence the correlation between ICB and GE is in Appendix B.

5 Discussion

Our results show that the ICB serves as a non-vacuous generalization bound, which we verified in the case of infinite-width networks. Furthermore, we performed a broader evaluation than is typically considered for theoretical GE bounds: i) We searched for ICB violations by evaluating ICB throughout training, rather than at a specific number of epochs or training loss value. ii) We varied the number of training samples and classification labels, compared to a static train/test split. iii) We considered robust GE in addition to standard GE. iv) Experiments were performed on five datasets. ICB was consistently satisfied at the expected

95% rate for models with at least $70 - 80\%$ test accuracy, which is encouraging since accurate models are more likely to be deployed in practice. It is, however, more helpful to threshold by training accuracy to establish a regime in which ICB always works well, since one does not assume access to held-out data when evaluating generalization bounds. The relationship between training accuracy and the percentage of models satisfying ICB was unfortunately weaker, despite being nearly 100% for overfitted models. Nonetheless, ICB was satisfied at a high rate of at least 92% of the time for three of five datasets (`MNIST`, `FashionMNIST`, and `EuroSAT`) without excluding any models by accuracy, and the training label randomization test was sensitive to tasks where ICB wasn't satisfied.

Compared to a simple training accuracy baseline, ICB performed well at ranking GE when the classification task was allowed to vary (e.g., grouping errors for 1 vs. 2 classification with those for a 2 vs. 3 task), or when the training accuracy was fixed at 100%. ICB, however, did not always outperform the training accuracy baseline for specific tasks and when GEs took a large range. However, a limited error ranking ability is not necessarily disqualifying for a generalization bound. It is unclear to what extent a generalization bound *ought* to be able to rank GEs, given that it is by definition merely an upper bound on the error. For example, GEs of 1% and 29% are both compatible with a bound of 30%, which would contribute to a poor ranking in terms of Kendall's τ. When varying one metaparameter at a time—in particular the diagonal regularization coefficient—a strong monotonic relationship is observed between ICB and robust errors AWGN and FGSM.

Relevance to deep learning One should use caution before extrapolating our conclusions based on infinite-width networks to finite-width DNNs. The ability of infinite-width networks to approximate their finite-width counterparts is reduced with increasing training samples (Lee et al., 2019), regularization (Lee et al., 2020), and depth (Li et al., 2021). Nevertheless, the infinite-width framework has allowed us to demonstrate the practical relevance of the ICB for an exciting family of models as a first step. It has been argued that understanding generalization for shallow kernel learning models is essential to understanding generalization behaviour of deep networks. Kernel learning and deep learning share the ability to exactly fit their training sets yet still generalize well, a phenomenon that other bounds fail to explain (Belkin et al., 2018). We leave the study of ICB in the context of finite-width DNNs to future work, which may require alternative MI estimation techniques.

6 Related Work

Kernel-regression generalization error Canatar et al. (2021b) derived an analytical expression for the generalization MSE of kernel regression models using a replica method from statistical mechanics. Their predictions show excellent agreement with the empirical GE of NTK models on `MNIST` and `CIFAR` datasets as a function of the training sample size. Furthermore, their method is sensitive to differences in difficulty between similar classification tasks, e.g., showing that `MNIST` "0 vs. 1" digit classification is easier to learn than "8 vs. 9". (Canatar et al., 2021a) extend the method to predict out-of-distribution GE. An alternative method is the Leave-One-Out (LOO) error estimator (Lachenbruch, 1967). LOO is generally impractical for Deep Learning (DL) due to the computational requirement of training N DNNs on N different training sets. However, Bachmann et al. (2021) proposed a closed-form LOO estimator based on a kernel regression model trained on the complete training set once. Their estimator shows excellent agreement with test MSE and accuracy for a five-layer ReLU NTK model trained on `MNIST` and `CIFAR`. While Bachmann et al. averaged results over five training sets of size $500 - 20000$, we only draw a single training set of $250 - 2000$ samples for each set of metaparameters. Our choice was made to reflect a practical "small data" scenario, where GE has to be bounded using a modest set of labeled data. As a result, however, our GE and ICB estimates have greater variance than those of Bachmann et al. We used the infinite-width DNN limit for convenience and as a first step to assess the efficacy of ICB; we did not set out to find optimal generalization bounds for kernel regression. An advantage of ICB is that it only requires access to $I(X;Z)$—a black-box statistic applicable to a wide variety of models beyond kernel regression. Therefore, ICB may become increasingly relevant for DLs using MI estimators with different strengths and assumptions, e.g., with distributional constraints on weight matrices (Gabrié et al., 2018) or infinite-depth corrections (Li et al., 2021).

Generalization bounds for deep learning Dziugaite & Roy (2017) develop a PAC-Bayes GE bound and evaluated it on a `MNIST` binary classification task using the complete training set ($N_{\text{train}} = 55\,\text{k}$) and a

fully-connected NN with 2-3 layers and ReLU activations. Although their bound was non-vacuous ($\approx 20\%$), it was several times larger than the error estimated on held-out data ($< 1\%$). A comparison with our work is difficult, as we did not use finite-width DNNs. We showed that the ICB yields a smaller ($\approx 10\%$) bound from less than 2000 samples for several classification tasks. Zhou et al. (2019) proposed a PAC-Bayes generalization bound based on the compressed size of a DNN after pruning and quantization. They obtain a GE bound of 46% for MNIST and $96 - 98\%$ for ImageNet. The measure of compression used by Zhou et al. (2019) is distinct from input compression in terms of MI here. The bounds of Dziugaite & Roy and Zhou et al. concern model complexity, whereas ICB is based on data compression by the hidden layers. Both Dziugaite & Roy and Zhou et al. optimized their bounds for best results, whereas we used standard training procedures.

Generalization bounds from unlabeled data GE bounds or estimates may be obtained without directly estimating model complexity. Garg et al. (2021) leverage the so-called "early learning" phenomenon, whereby DNNs fit true labels before noisy labels, to develop a post-hoc GE bound. They validate their bound on NTK-based wide DNNs, CNNs, and LSTMs. In contrast to our work, the Garg et al. bound requires additional unlabeled data, that in practice, can be carved out from the training set. They assign random labels to the carved-out set, and augment the training set with this random data. Their bound is based on the empirical error computed on both the clean and random set. Empirically, Garg et al. (2021) show that it may be possible to maintain model accuracy when training on partially randomized labels in some settings by using weight decay or early stopping. Unfortunately, random labels reduce the task signal-to-noise ratio, $I(X;Y)$, and may be challenging to apply with unregularized models that nonetheless generalize well (Zhang et al., 2017). Jiang et al. (2022) observed that the disagreement of separately trained DNNs on *unlabeled* held-out datasets is similar to the disagreement of those models on a *labeled* held-out set. Their claim follows an empirical observation that deep ensembles are often well-calibrated, however, this calibration property may not always hold in important settings (Kirsch & Gal, 2022).

Information compression and generalization The MI $I(S;w)$ between the training data $S = (x, y)$ supplied as input to a stochastic learning algorithm and the weights w it outputs can also serve to bound GE (Xu & Raginsky, 2017; Achille & Soatto, 2018). Decomposing $I(S;w)$ into $I(w;x) + I(w;y|x)$, Harutyunyan et al. (2020) show that reducing the second term—the information w contain about the labels y beyond what can be inferred from x—is key to avoid unintended memorization. As a result, these works *optimize* MI bounds, whereas we seek to *measure* MI to evaluate a GE bound. Furthermore, Shwartz-Ziv & Alemi (2020)[Appendix C.7] evaluated $I(S;w)$ for infinite-width networks and found that it tends to infinity as the training time goes to infinity. Thus, a GE bound based on $I(S;w)$ is vacuous for these networks which nevertheless generalize well. Saxe et al. (2018) observed a lack of compression in ReLU networks and argued that compression must be unrelated to generalization in DNNs, since it is known that ReLU networks generalize well. However, their binning procedure based on Paninski (2003) involves metaparameters that influence entropy and MI estimation. Other works have studied input compression in linear regression (Chechik et al., 2005) and finite-width ReLU DNNs using adaptive binning estimators (Chelombiev et al., 2019). We use MI bounds free from such metaparameters and observe input compression regardless of the nonlinearity type, consistent with Shwartz-Ziv & Alemi (2020). We are excited about future work on input compression phenomena and the challenging case of finite-width DNNs.

7 Conclusion

We assessed the ICB along three performance axes: tightness, percentage of trials satisfying the bound, and correlation with GE. Empirical results show that input compression serves as a simple and effective generalization bound, complementing previous theory. Additionally, ICB can help pinpoint interesting failures of robust generalization that go undetected by standard generalization metrics. An important consequence of the ICB with respect to NAS is that *bigger is not necessarily better*, at least in terms of the information complexity of infinite-width networks. Equally important as the architecture are the metaparameters and training duration, all of which affect input compression. Consistent with Occam's razor, less information complexity—or more input compression—yields more performant models, reducing the upper bound on generalization error. We conclude that input compression, which is data-centric, is a more effective complexity metric than model-centric proxies like the number of parameters or depth.

References

Alessandro Achille and Stefano Soatto. Emergence of Invariance and Disentanglement in Deep Representations. *Journal of Machine Learning Research*, 19(50):1–34, 2018.

Lynton Ardizzone, Radek Mackowiak, Ullrich Köthe, and Carsten Rother. Exact Information Bottleneck with Invertible Neural Networks: Getting the Best of Discriminative and Generative Modeling. *arXiv:2001.06448 [cs, stat]*, 2020.

Anish Athalye, Nicholas Carlini, and David Wagner. Obfuscated Gradients Give a False Sense of Security: Circumventing Defenses to Adversarial Examples. In *International Conference on Machine Learning*, pp. 274–283, 2018.

Gregor Bachmann, Thomas Hofmann, and Aurelien Lucchi. Generalization Through the Lens of Leave-One-Out Error. 2021. doi: 10.48550/arXiv.2203.03443.

Mikhail Belkin, Siyuan Ma, and Soumik Mandal. To Understand Deep Learning We Need to Understand Kernel Learning. In *Proceedings of the 35th International Conference on Machine Learning*, pp. 541–549. PMLR, 2018.

Mikhail Belkin, Daniel Hsu, Siyuan Ma, and Soumik Mandal. Reconciling modern machine-learning practice and the classical bias–variance trade-off. *Proceedings of the National Academy of Sciences*, 116(32): 15849–15854, 2019. doi: 10.1073/pnas.1903070116.

Anthony J. Bell and Terrence J. Sejnowski. An information-maximization approach to blind separation and blind deconvolution. *Neural Comput.*, 7(6):1129–1159, 1995.

Battista Biggio and Fabio Roli. Wild patterns: Ten years after the rise of adversarial machine learning. In *Proceedings of the 2018 ACM SIGSAC Conference on Computer and Communications Security*, CCS '18, pp. 2154–2156, New York, NY, USA, 2018. Association for Computing Machinery. ISBN 978-1-4503-5693-0. doi: 10.1145/3243734.3264418.

Abdulkadir Canatar, Blake Bordelon, and Cengiz Pehlevan. Out-of-distribution generalization in kernel regression. *Advances in neural information processing systems*, 34:12600–12612, 2021a. doi: 10.48550/arXiv.2106.02261.

Abdulkadir Canatar, Blake Bordelon, and Cengiz Pehlevan. Spectral Bias and Task-Model Alignment Explain Generalization in Kernel Regression and Infinitely Wide Neural Networks. *Nature Communications*, 12(1): 2914, 2021b. ISSN 2041-1723. doi: 10.1038/s41467-021-23103-1.

Nicholas Carlini, Anish Athalye, Nicolas Papernot, Wieland Brendel, Jonas Rauber, Dimitris Tsipras, Ian Goodfellow, Aleksander Madry, and Alexey Kurakin. On evaluating adversarial robustness. *arXiv preprint arXiv:1902.06705*, 2019.

Gal Chechik, Amir Globerson, Naftali Tishby, and Yair Weiss. Information Bottleneck for Gaussian Variables. *Journal of Machine Learning Research*, 6(Jan):165–188, 2005.

Ivan Chelombiev, Conor Houghton, and Cian O'Donnell. Adaptive Estimators Show Information Compression in Deep Neural Networks. In *International Conference on Learning Representations*, 2019.

Thomas M Cover and Joy A Thomas. *Elements of Information Theory*. John Wiley & Sons, Inc., New York, 1991.

Gintare Karolina Dziugaite and Daniel M. Roy. Computing Nonvacuous Generalization Bounds for Deep (Stochastic) Neural Networks with Many More Parameters than Training Data. In *Uncertainty in Artificial Intelligence (UAI)*, 2017.

Gintare Karolina Dziugaite, Alexandre Drouin, Brady Neal, Nitarshan Rajkumar, Ethan Caballero, Linbo Wang, Ioannis Mitliagkas, and Daniel M Roy. In search of robust measures of generalization. In *Advances in Neural Information Processing Systems*, volume 33, pp. 11723–11733. Curran Associates, Inc., 2020.

Alhussein Fawzi, Seyed-Mohsen Moosavi-Dezfooli, and Pascal Frossard. Robustness of classifiers: From adversarial to random noise. In *Advances in Neural Information Processing Systems*, volume 29. Curran Associates, Inc., 2016.

Marylou Gabrié, Andre Manoel, Clément Luneau, jean barbier, Nicolas Macris, Florent Krzakala, and Lenka Zdeborová. Entropy and mutual information in models of deep neural networks. In *Advances in Neural Information Processing Systems 31*, pp. 1821–1831. Curran Associates, Inc., 2018.

Saurabh Garg, Sivaraman Balakrishnan, Zico Kolter, and Zachary Lipton. RATT: Leveraging unlabeled data to guarantee generalization. In *Proceedings of the 38th International Conference on Machine Learning*, volume 139 of *Proceedings of Machine Learning Research*, pp. 3598–3609. PMLR, 2021.

Justin Gilmer, Nicolas Ford, Nicholas Carlini, and Ekin Cubuk. Adversarial Examples Are a Natural Consequence of Test Error in Noise. In *Proceedings of the 36th International Conference on Machine Learning*, pp. 2280–2289. PMLR, 2019.

Ziv Goldfeld, Ewout Van Den Berg, Kristjan Greenewald, Igor Melnyk, Nam Nguyen, Brian Kingsbury, and Yury Polyanskiy. Estimating Information Flow in Deep Neural Networks. In *Proceedings of the 36th International Conference on Machine Learning*, volume 97 of *Proceedings of Machine Learning Research*, pp. 2299–2308. PMLR, 2019.

Ian. J. Goodfellow, Jonathon. Shlens, and Christian. Szegedy. Explaining and Harnessing Adversarial Examples. In *International Conference on Learning Representations*, 2015.

Hrayr Harutyunyan, Kyle Reing, Greg Ver Steeg, and Aram Galstyan. Improving generalization by controlling label-noise information in neural network weights. In *Proceedings of the 37th International Conference on Machine Learning*, volume 119 of *Proceedings of Machine Learning Research*, pp. 4071–4081. PMLR, 2020.

Patrick Helber, Benjamin Bischke, Andreas Dengel, and Damian Borth. Introducing EuroSAT: A novel dataset and deep learning benchmark for land use and land cover classification. In *IGARSS 2018-2018 IEEE International Geoscience and Remote Sensing Symposium*, pp. 204–207, 2018.

Patrick Helber, Benjamin Bischke, Andreas Dengel, and Damian Borth. Eurosat: A novel dataset and deep learning benchmark for land use and land cover classification. *IEEE Journal of Selected Topics in Applied Earth Observations and Remote Sensing*, 2019.

Jörn-Henrik Jacobsen, Arnold W. M. Smeulders, and Edouard Oyallon. I-RevNet: Deep Invertible Networks. In *International Conference on Learning Representations*, 2018.

Arthur Jacot, Franck Gabriel, and Clement Hongler. Neural tangent kernel: Convergence and generalization in neural networks. In *Advances in Neural Information Processing Systems 31*, pp. 8571–8580. Curran Associates, Inc., 2018.

Yiding Jiang*, Behnam Neyshabur*, Hossein Mobahi, Dilip Krishnan, and Samy Bengio. Fantastic Generalization Measures and Where to Find Them. In *International Conference on Learning Representations*, 2019.

Yiding Jiang, Parth Natekar, Manik Sharma, Sumukh K. Aithal, Dhruva Kashyap, Natarajan Subramanyam, Carlos Lassance, Daniel M. Roy, Gintare Karolina Dziugaite, Suriya Gunasekar, Isabelle Guyon, Pierre Foret, Scott Yak, Hossein Mobahi, Behnam Neyshabur, and Samy Bengio. Methods and Analysis of The First Competition in Predicting Generalization of Deep Learning. In *Proceedings of the NeurIPS 2020 Competition and Demonstration Track*, pp. 170–190. PMLR, 2021.

Yiding Jiang, Vaishnavh Nagarajan, Christina Baek, and J Zico Kolter. Assessing generalization of SGD via disagreement. In *International Conference on Learning Representations*, 2022.

Andreas Kirsch and Yarin Gal. A note on "Assessing Generalization of SGD via Disagreement". *arXiv:2202.01851*, abs/2202.01851, 2022.

Alex Krizhevsky. Learning multiple layers of features from tiny images. Technical report, 2009.

P. A. Lachenbruch. An almost unbiased method of obtaining confidence intervals for the probability of misclassification in discriminant analysis. *Biometrics*, 23(4):639–645, 1967. ISSN 0006-341X.

Yann LeCun and Corinna Cortes. The MNIST Database of Handwritten Digits. *http://yann.lecun.com/exdb/mnist/*, 1998.

Jaehoon Lee, Lechao Xiao, Samuel Schoenholz, Yasaman Bahri, Roman Novak, Jascha Sohl-Dickstein, and Jeffrey Pennington. Wide neural networks of any depth evolve as linear models under gradient descent. In *Advances in Neural Information Processing Systems 32*, pp. 8570–8581. Curran Associates, Inc., 2019.

Jaehoon Lee, Samuel Schoenholz, Jeffrey Pennington, Ben Adlam, Lechao Xiao, Roman Novak, and Jascha Sohl-Dickstein. Finite versus infinite neural networks: An empirical study. In *Advances in Neural Information Processing Systems*, volume 33, pp. 15156–15172. Curran Associates, Inc., 2020.

Mufan Bill Li, Mihai Nica, and Daniel M. Roy. The Future is Log-Gaussian: ResNets and Their Infinite-Depth-and-Width Limit at Initialization. In *Advances in Neural Information Processing Systems*, 2021.

Kevin P. Murphy. *Machine Learning: A Probabilistic Perspective*. MIT Press, 2012.

Yuval Netzer, Tao Wang, Adam Coates, Alessandro Bissacco, Bo Wu, and Andrew Y Ng. Reading Digits in Natural Images with Unsupervised Feature Learning. In *NIPS Workshop on Deep Learning and Unsupervised Feature Learning*, 2011.

Behnam Neyshabur, Ryota Tomioka, and Nathan Srebro. Norm-Based Capacity Control in Neural Networks. In *Proceedings of The 28th Conference on Learning Theory*, 2015.

Roman Novak, Lechao Xiao, Jiri Hron, Jaehoon Lee, Alexander A. Alemi, Jascha Sohl-Dickstein, and Samuel S. Schoenholz. Neural tangents: Fast and easy infinite neural networks in python. In *International Conference on Learning Representations*, 2020.

Liam Paninski. Estimation of Entropy and Mutual Information. In *Neural Computation*, volume 15, pp. 1191–1253. 2003.

Ben Poole, Sherjil Ozair, Aaron Van Den Oord, Alex Alemi, and George Tucker. On Variational Bounds of Mutual Information. In *Proceedings of the 36th International Conference on Machine Learning*, volume 97 of *Proceedings of Machine Learning Research*, pp. 5171–5180. PMLR, 2019.

Andrew Michael Saxe, Yamini Bansal, Joel Dapello, Madhu Advani, Artemy Kolchinsky, Brendan Daniel Tracey, and David Daniel Cox. On the Information Bottleneck Theory of Deep Learning. In *International Conference on Learning Representations*, 2018.

Ravid Shwartz-Ziv. Information Flow in Deep Neural Networks. 2022. doi: 10.48550/arXiv.2202.06749.

Ravid Shwartz-Ziv and Alexander A Alemi. Information in infinite ensembles of infinitely-wide neural networks. In *Proceedings of the 2nd Symposium on Advances in Approximate Bayesian Inference*, volume 118 of *Proceedings of Machine Learning Research*, pp. 1–17. PMLR, 2020.

Ravid Shwartz-Ziv, Amichai Painsky, and Naftali Tishby. Representation Compression and Generalization in Deep Neural Networks. *OpenReview*, 2019.

D. J. Strouse and David J. Schwab. The deterministic information bottleneck. In *Uncertainty in Artificial Intelligence (UAI)*, 2016.

Christian Szegedy, Wojciech Zaremba, Ilya Sutskever, Joan Bruna, Dumitru Erhan, Ian Goodfellow, and Rob Fergus. Intriguing properties of neural networks. In *International Conference on Learning Representations*, 2014.

Naftali Tishby. Information Theory of Deep Learning, 2017. URL `https://youtu.be/bLqJHjXihK8?t=1051`.

Dimitris Tsipras, Shibani Santurkar, Logan Engstrom, Alexander Turner, and Aleksander Madry. Robustness May Be at Odds with Accuracy. In *International Conference on Learning Representations*, 2019.

Aaron van den Oord, Yazhe Li, and Oriol Vinyals. Representation Learning with Contrastive Predictive Coding. 2018. doi: 10.48550/arXiv.1807.03748.

Han Xiao, Kashif Rasul, and Roland Vollgraf. Fashion-MNIST: A novel image dataset for benchmarking machine learning algorithms, 2017.

Aolin Xu and Maxim Raginsky. Information-theoretic analysis of generalization capability of learning algorithms. In *Advances in Neural Information Processing Systems*, volume 30. Curran Associates, Inc., 2017.

Chiyuan Zhang, Samy Bengio, Moritz Hardt, Benjamin Recht, and Oriol Vinyals. Understanding deep learning requires rethinking generalization. In *International Conference on Learning Representations*, 2017.

Chiyuan Zhang, Samy Bengio, Moritz Hardt, Benjamin Recht, and Oriol Vinyals. Understanding deep learning (still) requires rethinking generalization. *Communications of the ACM*, 64(3):107–115, 2021. ISSN 0001-0782. doi: 10.1145/3446776.

Wenda Zhou, Victor Veitch, Morgane Austern, Ryan P. Adams, and Peter Orbanz. Non-vacuous Generalization Bounds at the ImageNet Scale: A PAC-Bayesian Compression Approach. In *International Conference on Learning Representations*, 2019.

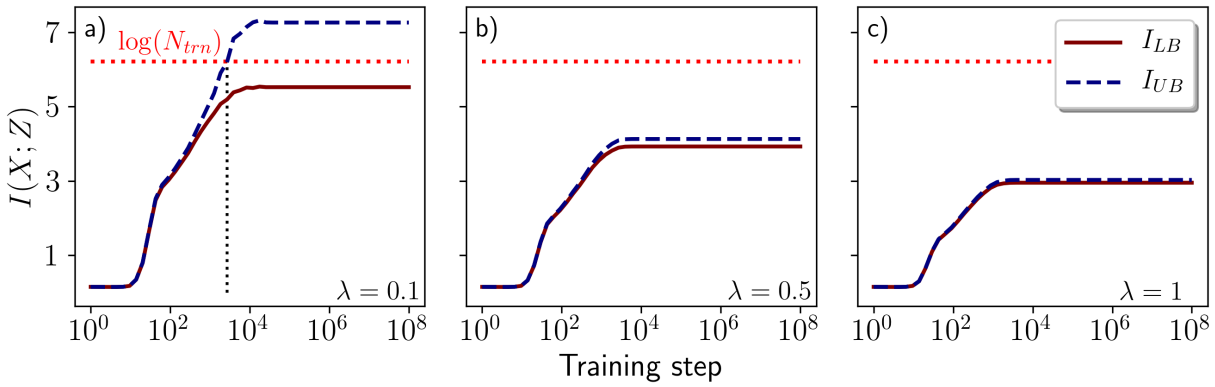

Figure 5: We plot $I(X;Z)$ upper (2) and lower (5) bounds corresponding to the illustrative `EuroSAT` example (Figure 1). Increasing the regularization to $\lambda = 0.5$ in b) and $\lambda = 1.0$ in c) reduces MI below $\log(N_{\text{trn}})$. Samples to the right of the vertical line in a) where I_{UB} crosses $\log(N_{\text{trn}})$ are discarded for the main analyses. NB: We use natural units ("Nats" or "Shannons") for $I(X;Z)$ here, but we convert to bits when evaluating the ICB.

A Appendix

A.1 Assumptions of input compression bound

It is assumed in the construction of the ICB that X is a d-dimensional random variable that obeys an ergodic MRF probability distribution, asymptotically in d. A MRF is an undirected graphical model, used to model data distributions with a particular conditional independency structure, which is commonly used for spatial data, including images (see Murphy (2012)[Chapter 19] for an excellent introduction). Mathematically, this means that $p(x)$ factorizes into a product of terms which represent the potentials for each clique on the underlying graph. In terms of correlations, this means that each pixel is strongly correlated with its immediate neighbors, but not with pixels that are further away. The "ergodic" part is essential for the derivation of the ICB: An ergodic MRF does not "get stuck" in any part of the state space; in other words, there is a nonzero probability for every possible state to be reached. Ultimately, this is the necessary assumption to invoke the Asymptotic Equipartition Property (AEP), which in turn allows us invoke typicality. Defining the typical set is the crux of the ICB derivation, because it enables us to quantify the hypothesis space cardinality in terms of entropy. From here, the rest follows from information-theory fundamentals.

A.2 Lower bound on MI

We may lower bound $I(X;Z)$ using a bound of similar form as equation 2 based on a batch of N samples:

$$I(X;Z) \geq \mathbb{E}\left[\frac{1}{N}\sum_{i=1}^{N}\log\frac{p(z_i|x_i)}{\frac{1}{N}\sum_j p(z_i|x_j)}\right] = I_{\text{LB}}\,, \tag{5}$$

where the expectation is taken over N independent samples from the joint distribution $\prod_j p(x_j, z_j)$. The main difference between this bound and equation 5 is the inclusion of $p(z_i|x_i)$ in the denominator.

A.3 Illustrative example and filtering MI

We empirically verified that equation 5 and equation 2 yield similar results when $I_{\text{UB}} < \log(N_{\text{trn}})$ (Fig. A5).

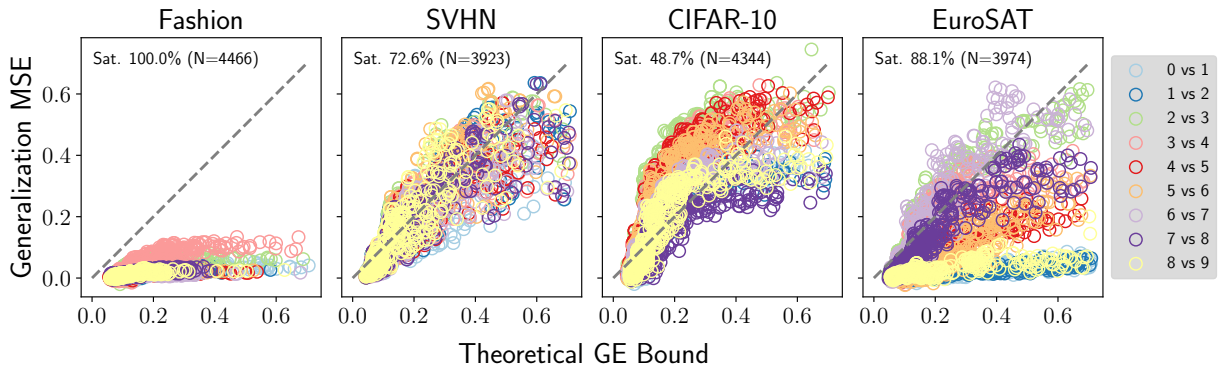

Figure 6: ICB is plotted versus GE for `FashionMNIST`, `SVHN`, `CIFAR-10`, and `EuroSAT` datasets. The ICB satisfaction rate is annotated in the top left corner of each plot with format "ICB % (N)". Each binary classification task is assigned a unique colour to highlight inter-task differences in ICB satisfaction rate. See Figure 2 of §4.1 for the corresponding Figure with GE expressed in terms of classification error rather than MSE. NB: Results for `MNIST` omitted from Figure as they were similar to `FashionMNIST`.

A.4 Bounding generalization throughout training

Loss function We considered GE in terms of MSE in addition to classification error (Fig. A6). This change results in no difference in the overall ICB Sat. for `FashionMNIST`, an improvement for `SVHN` from 44.5% to 72.6%, and a small decrease for `CIFAR-10` from to 59.3% to 48.7% as well as for `EuroSAT` from 93.6% to 88.1%.

Activation function Overall, `ReLU` networks satisfied ICB more frequently than `Erf` networks (Table A11).

The following caption applies to Tables A6-10.

Kendall's τ ranking for three generalization error types: Clean, AWGN and FGSM by training accuracy "Train (baseline)" and ICB are presented. One hundred random seeds are used to draw different metaparameters uniform random for each task, for which models are evaluated five (5) times each during training resulting in a maximum of 500 samples per task. The number of valid samples out of 500, i.e., those with $I_{\text{UB}}(X;Z) \leq \log(N_{\text{train}})$ is indicated in the N_{valid} column. ICB % indicates the percentage of samples that satisfy the ICB, i.e., `Clean generalization error` $\leq$ `ICB`. Entries in the "Row average" row are obtained by simply averaging across the nine (9) tasks. Kendall's τ values for the "Overall" row may differ substantially from "Row average" as this corresponds to aggregating all raw data points and considering them as one task before calculating τ. **Bold** is used to denote whether the baseline or ICB achieve a better ranking of generalization errors.

A.5 Bounding generalization at steady state

Results for bounding the generalization error at steady state are summarized in Table A11.

A.6 Advantage of ICB versus MI

To gain further insight into ICB, we examine GEs for a specific `CIFAR-10` binary classification task (classes 2 and 5) using three different training set sizes. Plotting GEs with respect to $I(X;Z)$ alone yields a poor overall ranking, whereas ICB effectively aligns trials with different training set sizes (Figure 13).

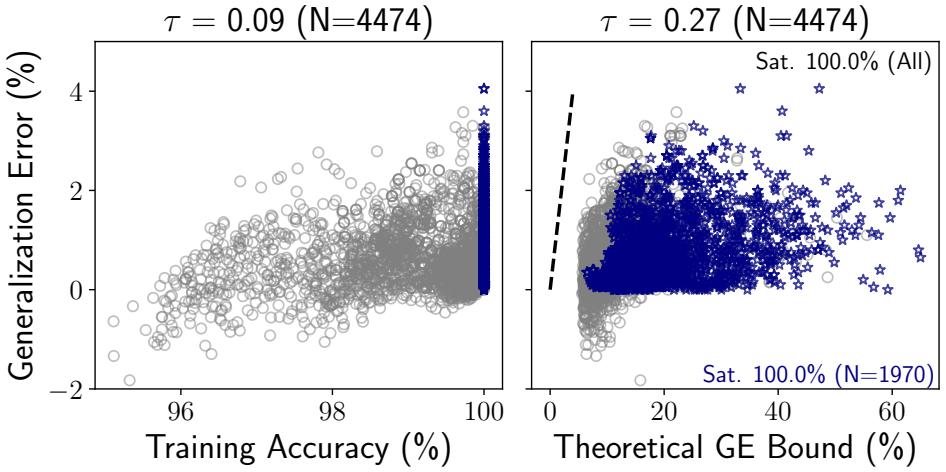

(a)

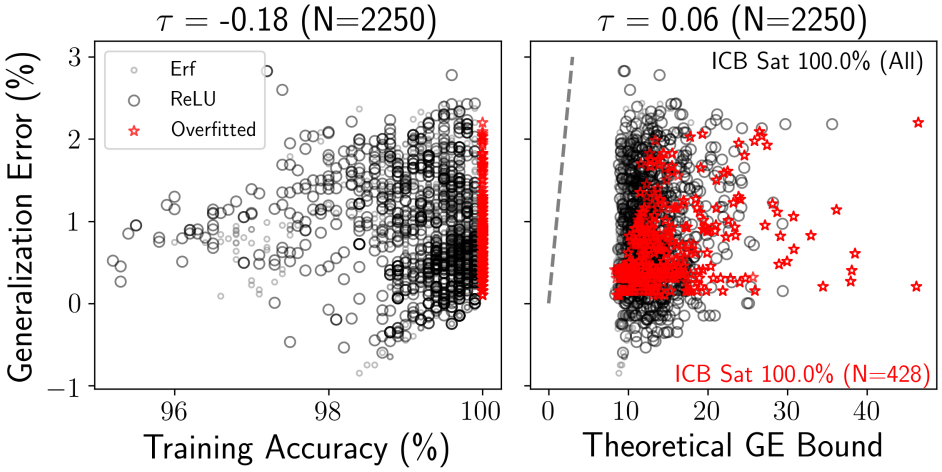

(b)

Figure 7: a) MNIST models evaluated throughout training, b) models evaluated at steady state $t = \infty$.

Table 6: Kendall's τ ranking for `MNIST`. See complete caption in §A.4.

Details			Train (baseline)			ICB		
Task	N_{valid}	ICB %	Clean	AWGN	FGSM	Clean	AWGN	FGSM
0 vs. 1	499	100%	0.36	0.37	0.35	0.10	0.09	0.10
1 vs. 2	498	100%	0.39	0.65	0.33	0.34	0.52	0.32
2 vs. 3	497	100%	0.42	0.57	0.46	0.42	0.55	0.46
3 vs. 4	500	100%	0.27	0.32	0.24	0.22	0.29	0.23
4 vs. 5	493	100%	0.19	0.31	0.14	0.19	0.32	0.17
5 vs. 6	497	100%	0.49	0.59	0.51	0.44	0.53	0.46
6 vs. 7	498	100%	0.29	0.27	0.23	0.17	0.23	0.17
7 vs. 8	498	100%	0.35	0.44	0.32	0.38	0.46	0.38
8 vs. 9	494	100%	0.42	0.56	0.44	0.38	0.52	0.42
Row average		100%	**0.35**	**0.45**	**0.34**	0.29	0.39	0.30
Overall			0.09	0.12	0.03	**0.27**	**0.31**	**0.24**

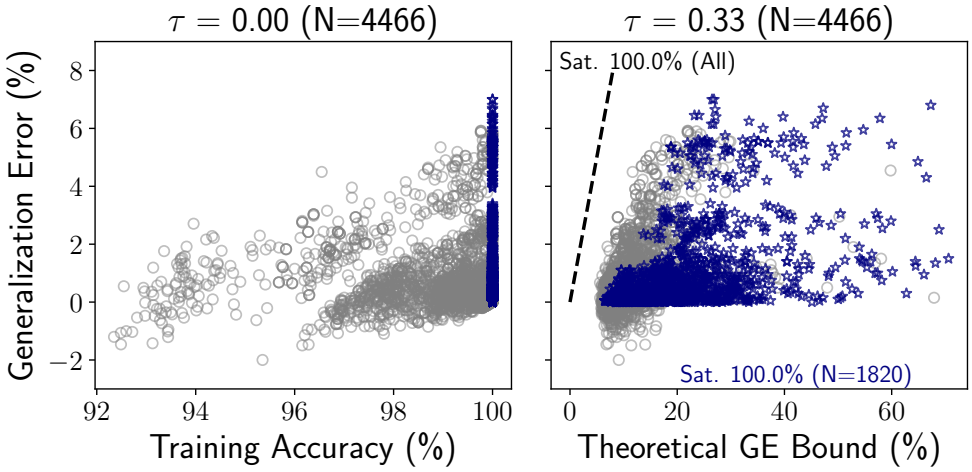

(a)

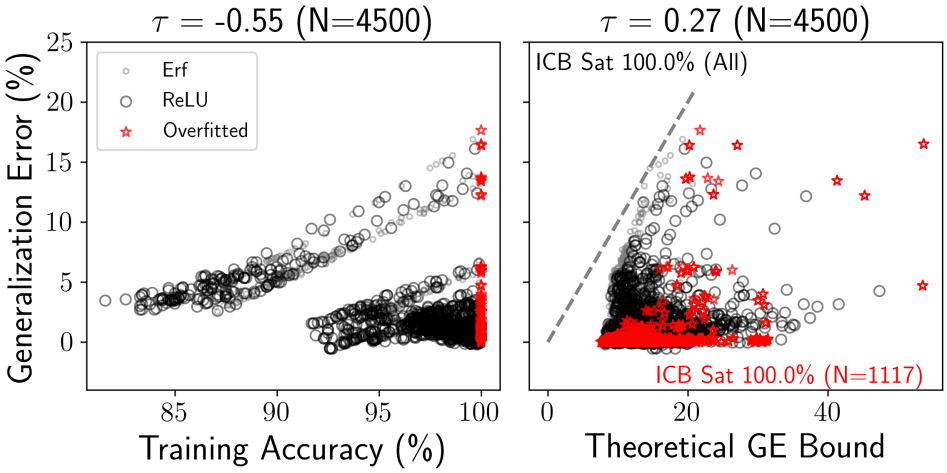

(b)

Figure 8: FashionMNIST models evaluated a) throughout training and b) at steady state $t = \infty$.

Table 7: Kendall's τ ranking for `FashionMNIST`. See complete caption in §A.4.

Details			Train (baseline)			ICB		
Task	N_{valid}	ICB %	Clean	AWGN	FGSM	Clean	AWGN	FGSM
0 vs. 1	250	100%	0.59	0.67	0.66	0.46	0.57	0.54
1 vs. 2	248	100%	0.48	0.59	0.55	0.42	0.50	0.46
2 vs. 3	247	100%	0.76	0.80	0.80	0.57	0.60	0.61
3 vs. 4	243	100%	0.78	0.82	0.84	0.67	0.66	0.66
4 vs. 5	250	100%	0.04	-0.02	-0.11	0.08	-0.02	0.00
5 vs. 6	249	100%	0.18	0.15	0.04	0.13	0.17	0.06
6 vs. 7	250	100%	0.35	0.26	0.23	0.17	0.16	0.12
7 vs. 8	250	100%	0.37	0.52	0.31	0.35	0.46	0.35
8 vs. 9	250	100%	0.40	0.29	0.38	0.20	0.11	0.20
Row average		100%	**0.44**	**0.45**	**0.41**	0.34	0.35	0.34
Overall			-0.02	-0.03	-0.09	**0.33**	**0.33**	**0.31**

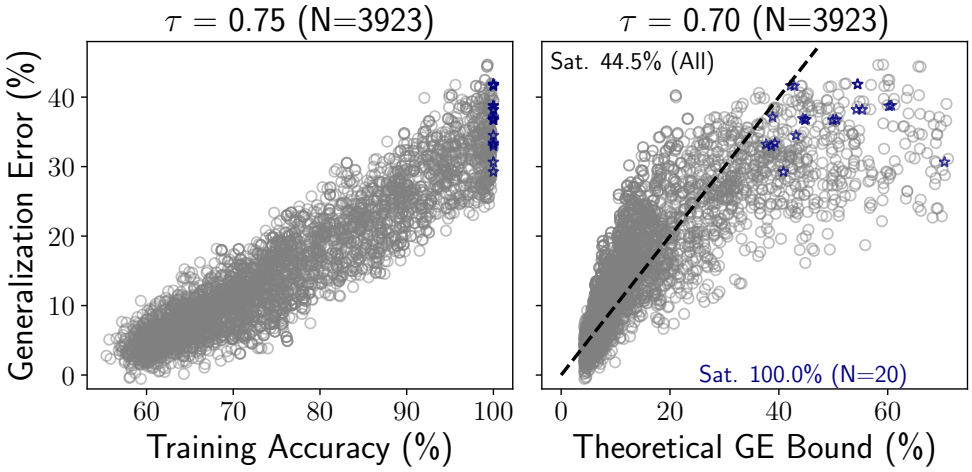

(a)

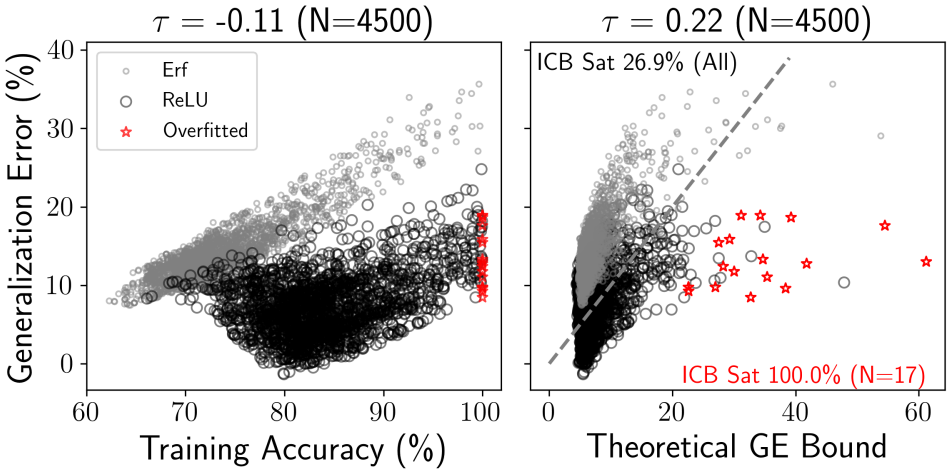

(b)

Figure 9: a) SVHN models evaluated throughout training, b) models evaluated at steady state $t = \infty$.

Table 8: Kendall's τ ranking for `SVHN`. See complete caption in §A.4.

Details			Train (baseline)			ICB		
Task	N_{valid}	ICB %	Clean	AWGN	FGSM	Clean	AWGN	FGSM
0 vs. 1	443	71%	0.75	0.85	0.80	0.70	0.74	0.63
1 vs. 2	432	33%	0.81	0.90	0.84	0.74	0.73	0.66
2 vs. 3	440	34%	0.82	0.89	0.83	0.74	0.73	0.64
3 vs. 4	438	44%	0.82	0.90	0.83	0.73	0.75	0.67
4 vs. 5	441	60%	0.81	0.90	0.83	0.76	0.75	0.65
5 vs. 6	442	25%	0.86	0.92	0.86	0.73	0.72	0.65
6 vs. 7	429	49%	0.79	0.90	0.83	0.72	0.71	0.63
7 vs. 8	440	48%	0.78	0.88	0.83	0.73	0.73	0.65
8 vs. 9	438	32%	0.84	0.91	0.82	0.74	0.73	0.63
Row average		44%	**0.81**	**0.89**	**0.83**	0.73	0.73	0.65
Overall			**0.75**	**0.85**	**0.80**	0.71	0.72	0.64

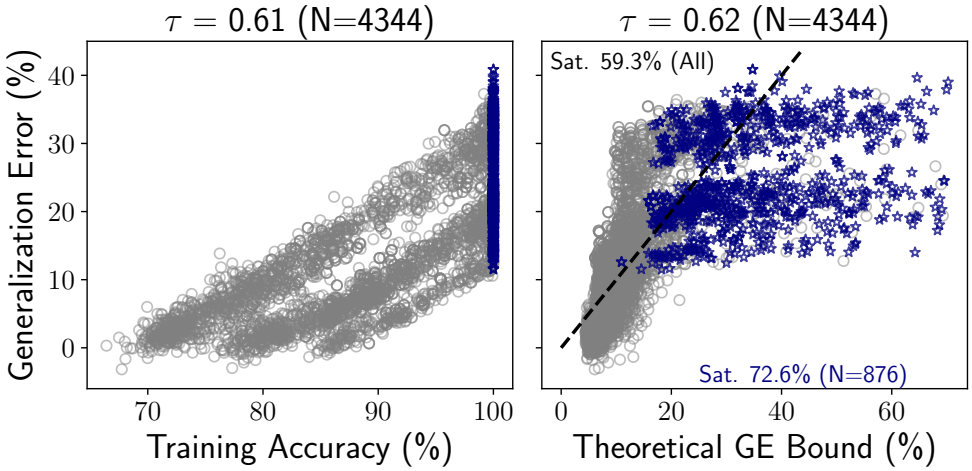

(a)

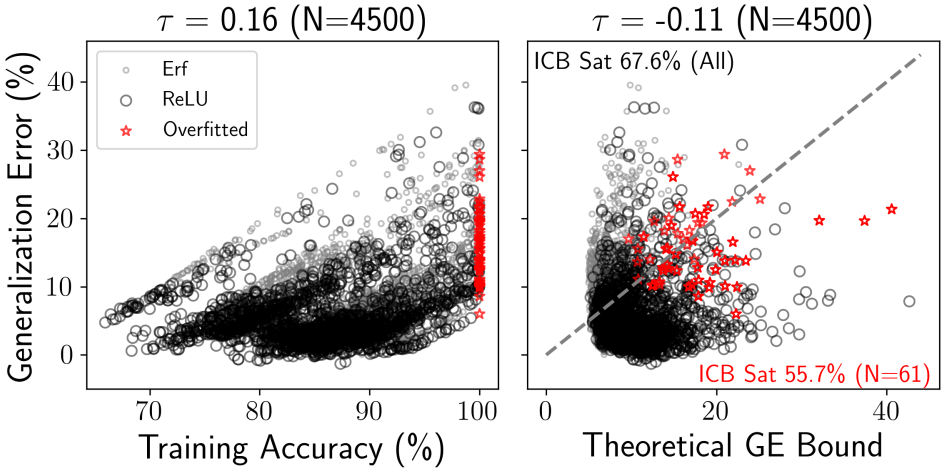

(b)

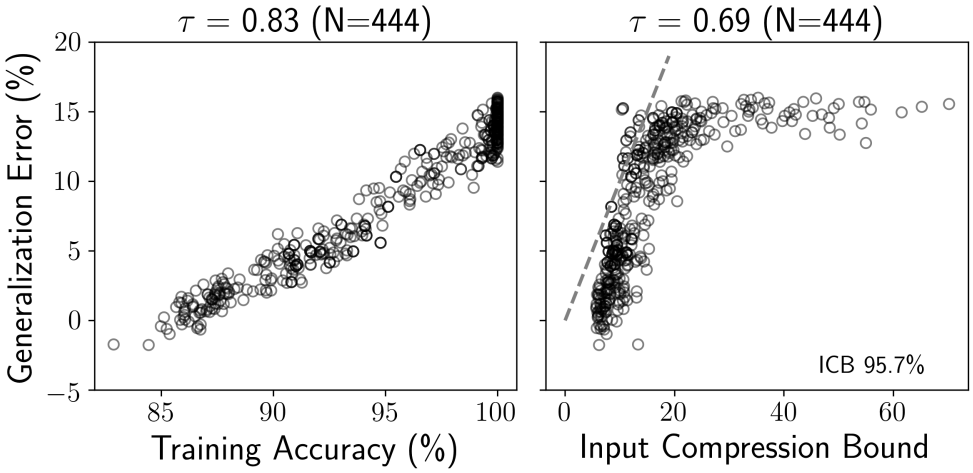

(c)

Figure 10: a) CIFAR models evaluated throughout training, b) models evaluated at steady state $t = \infty$, c) select models from a) with $\geq 84\%$ test accuracy.

Table 9: Kendall's τ ranking for `CIFAR-10`. See complete caption in §A.4.

Details			Train (baseline)			ICB		
Task	N_{valid}	ICB %	Clean	AWGN	FGSM	Clean	AWGN	FGSM
0 vs. 1	482	74%	0.85	0.88	0.87	0.72	0.73	0.69
1 vs. 2	489	79%	0.84	0.87	0.87	0.75	0.75	0.70
2 vs. 3	487	29%	0.88	0.90	0.86	0.77	0.76	0.68
3 vs. 4	480	35%	0.86	0.88	0.85	0.76	0.76	0.69
4 vs. 5	472	39%	0.89	0.90	0.87	0.76	0.75	0.68
5 vs. 6	481	41%	0.86	0.89	0.86	0.76	0.75	0.67
6 vs. 7	487	68%	0.82	0.85	0.84	0.78	0.77	0.70
7 vs. 8	488	97%	0.82	0.86	0.84	0.71	0.71	0.66
8 vs. 9	486	74%	0.85	0.88	0.87	0.75	0.74	0.71
Row average		59%	**0.85**	**0.88**	**0.86**	0.75	0.75	0.69
Overall			0.61	0.65	**0.64**	**0.62**	0.65	0.62

Table 10: Kendall's τ ranking for `EuroSAT`. See complete caption in §A.4.

Details			Train (baseline)			ICB		
Task	N_{valid}	ICB %	Clean	AWGN	FGSM	Clean	AWGN	FGSM
0 vs. 1	414	100%	0.26	0.40	0.37	0.25	0.43	0.38
1 vs. 2	389	100%	0.30	0.59	0.50	0.24	0.54	0.37
2 vs. 3	468	68%	0.86	0.91	0.76	0.77	0.78	0.60
3 vs. 4	490	97%	0.86	0.86	0.83	0.72	0.72	0.65
4 vs. 5	485	100%	0.62	0.61	0.77	0.70	0.70	0.68
5 vs. 6	444	100%	0.78	0.79	0.80	0.68	0.67	0.62
6 vs. 7	475	72%	0.89	0.88	0.80	0.74	0.74	0.62
7 vs. 8	467	100%	0.80	0.83	0.82	0.77	0.77	0.67
8 vs. 9	335	100%	0.47	0.74	0.63	0.40	0.61	0.51
Row average		93%	**0.65**	**0.73**	**0.70**	0.59	0.66	0.57
Overall			**0.34**	**0.36**	**0.33**	0.26	0.28	0.28

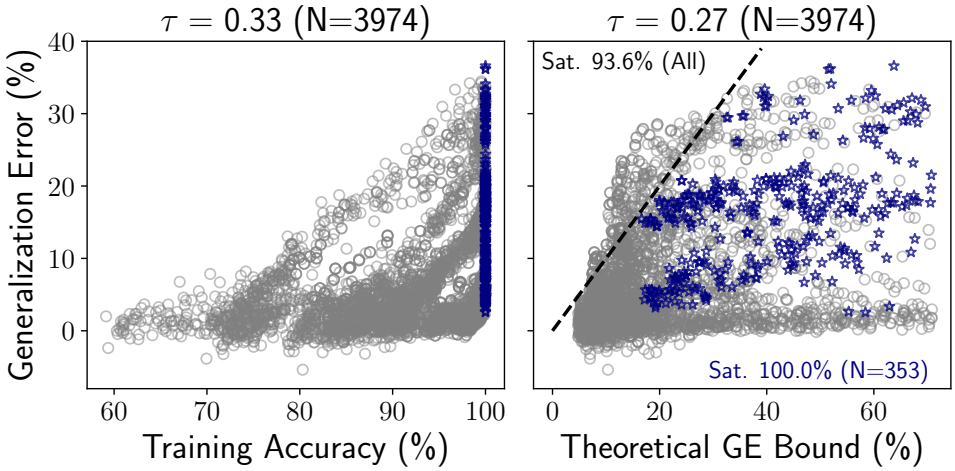

(a)

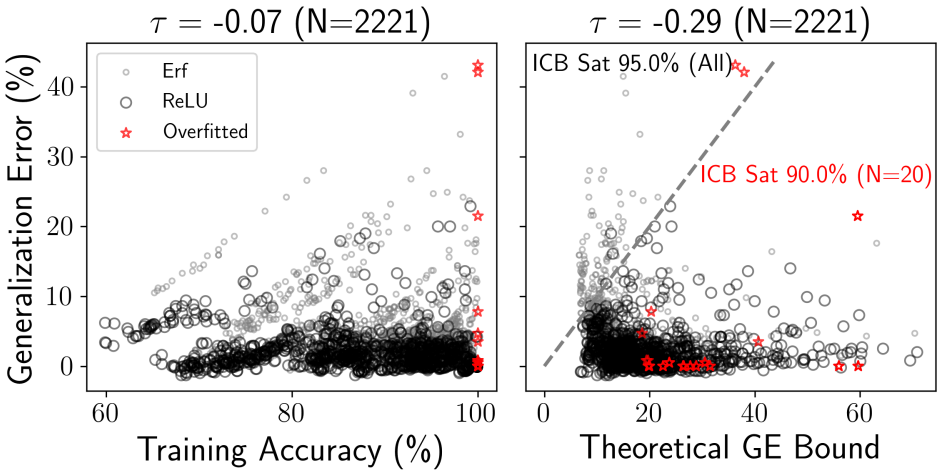

(b)

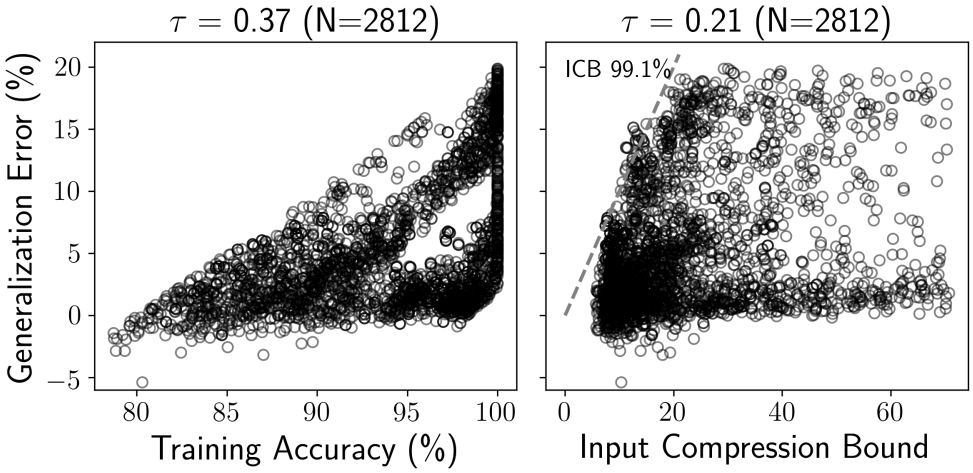

(c)

Figure 11: a) EuroSAT model evaluated throughout training, b) models evaluated at steady state $t = \infty$, c) select models from a) with $\geq 80\%$ test accuracy.

Table 11: **Results for bounding generalization error across five (5) datasets with Input Compression Bound (ICB).** For each dataset, all $\binom{10}{2} = 45$ binary label combinations are evaluated for $S = 25 - 50$ meta-parameter combinations drawn uniform random. The ICB % column indicates the percentage of N_{trials} that satisfy the ICB, where $N_{\text{trials}} = \binom{10}{2} \times S$. The mean and maximum Clean generalization error is indicated by "Mean Err" and "Max Err" respectively. The training set sample size is indicated by N_{train}. A test set with $N_{\text{test}} = 2000$ is used in all cases except for `EuroSAT` ($N_{\text{test}} = 1000$). Results are broken down by nonlinearity type as `Erf` resulted in ICB being satisfied less often.

					Error	
Dataset	N_{train}	N_{trials}	Arch	ICB %	Mean Err	Max Err
`MNIST`	1000	1125	`Erf`	100.0	0.8	2.4
			`ReLU`	100.0	0.8	2.8
`Fashion`	1000	2250	`Erf`	99.9	1.3	16.5
			`ReLU`	100.0	1.4	17.7
`SVHN`	2000	2250	`Erf`	0.3	14.1	35.7
			`ReLU`	52.8	7.4	24.8
`CIFAR-10`	2000	2250	`Erf`	47.6	8.5	39.5
			`ReLU`	86.5	5.4	36.3
`EuroSAT`	1000	1125	`Erf`	90.0	2.1	22.9
			`ReLU`	99.5	5.1	43.0

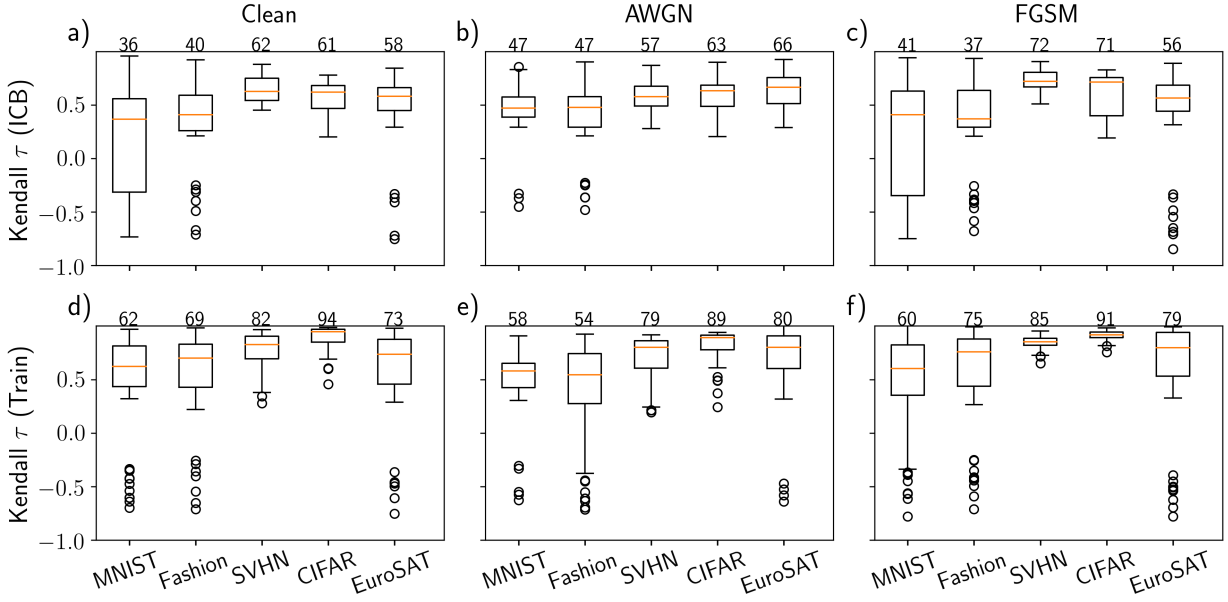

Figure 12: Boxplots show the Kendall τ ranking between: a,d) Clean, b,e) AWGN, and c,f) FGSM GEs and ICB (*top row*) compared to a training accuracy baseline (*bottom row*). We discard τ values with corresponding $p > 0.05$. The median τ value is annotated above each box and multiplied by 100 for ease of interpretation.

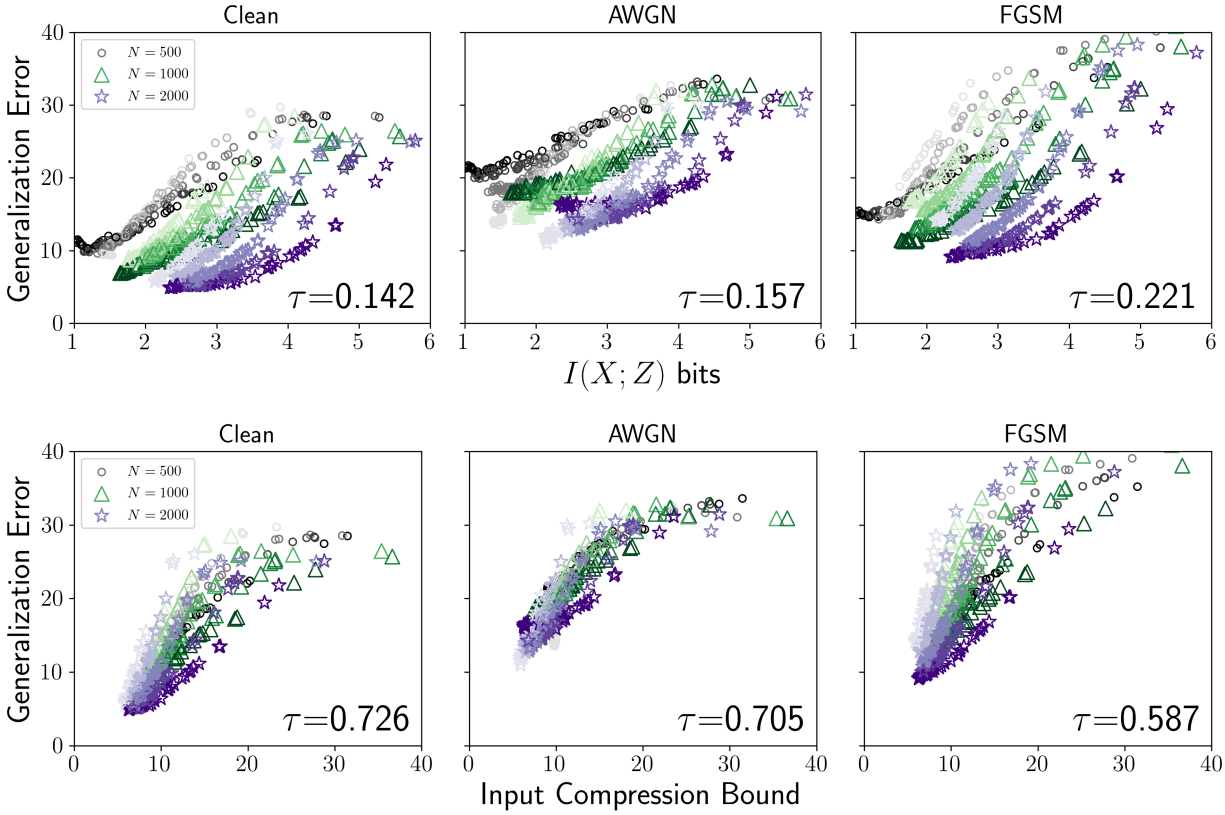

Figure 13: **ICB (bottom) ranks GEs better than $I(X;Z)$ alone (top) for different training set sizes.** Shown are 750 fully-connected NTK ReLU models trained ($t = \infty$) on a `CIFAR-10` binary classification task (classes 2 and 5) using three different training set sizes of $N = \{500, 1000, 2000\}$ and a test set with $N = 2000$. For each training set, 250 meta-parameter combinations are drawn from a uniform random distribution (see §3.2 for details). Model depth is indicated by the colour intensity for each series, where the darkest shade indicates the maximum depth of five (5) layers. Three GE types are evaluated: `Clean` (standard), AWGN (adversarial), and FGSM (adversarial) are plotted with respect to $I(X;Z)$ (*top row*) and ICB (*bottom row*). Plotting GE versus the ICB better aligns results for different sized training sets (N) compared to $I(X;Z)$, and yields a better ranking in terms of Kendall-τ.

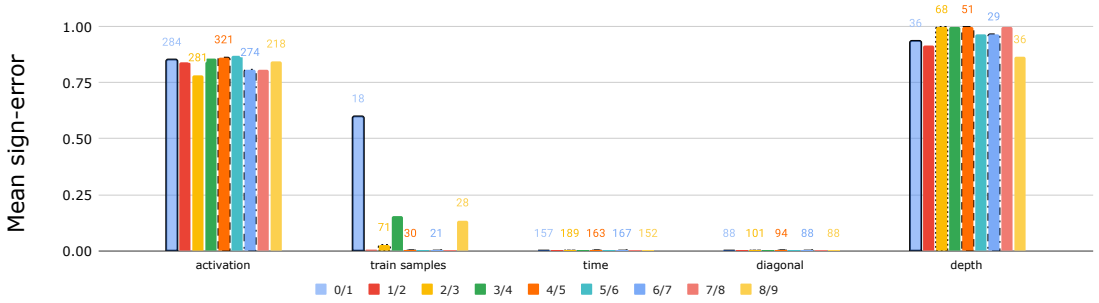

(a)

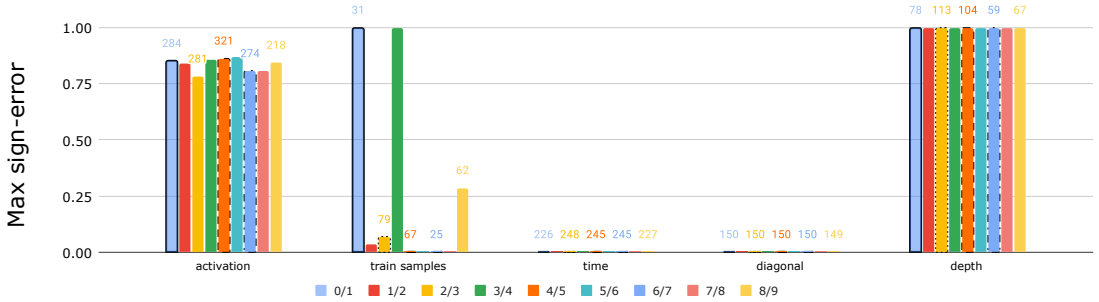

(b)

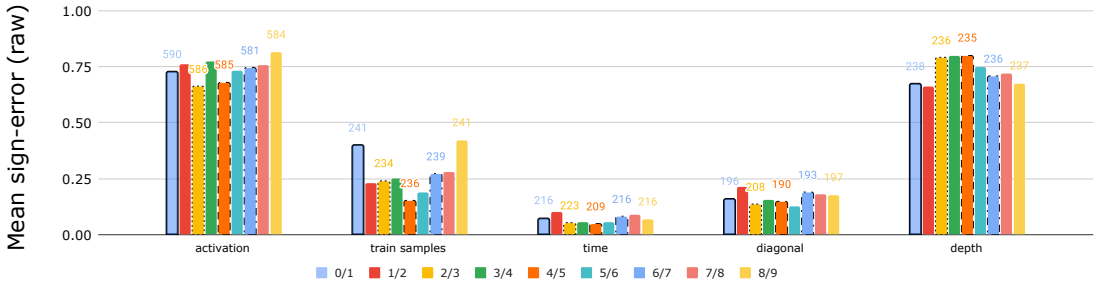

(c)

Figure 14: GE prediction sign-errors for five different metaparameter interventions on nine CIFAR-10 binary classification tasks $\{0$ vs. $1, 1$ vs. $2, \ldots, 8$ vs. $9\}$. Plots a), b) discard samples where differences in GE are too small to reliably measure (see text for details), whereas c) shows the unfiltered data for comparison. Plots a), c) report mean sign-error, whereas b reports the maximum or "robust" sign-error across all assignments of each metaparameter. See Table 12 for a detailed worked example showing how a column is computed in these plots.

B Metaparameter study

We perform *coupled-network* experiments as per Dziugaite et al. (2020) to assess the ability of ICB to predict an increase or decrease of GE for specific metaparameter interventions (Figure 14). For this experiment we select metaparameters identically as in Exp. A, only instead of sampling the number of train set samples $\mathcal{U}(250, 2000)$, we chose five values: $1000, 1250, 1500, 1750, 2000$. For each of nine binary classification tasks, we train models with 1250 metaparameter settings consisting of five different: depths, diagonal regularization values, train set samples, and train times; and the two activation functions. We subsequently assess Sign-Error (SE) (equation 6) for all possible combinations of the numerical metaparameters (example shown in Table 12).

$$\mathrm{SE}(P^e, \mathrm{ICB}) = \frac{1}{2}\mathbb{E}_{(w,w')\sim P^e}\left[1 - \mathrm{sgn}\left(\mathrm{GE}\left(w'\right) - \mathrm{GE}\left(w\right)\right) \cdot \mathrm{sgn}\left(\mathrm{ICB}\left(w'\right) - \mathrm{ICB}\left(w\right)\right)\right]. \tag{6}$$

The SE is evaluated with respect to different assignments of the metaparameters, w and w', which are said to be drawn from an environment e and differ in only one metaparameter value. Note that in Dziugaite et al. the expectation in equation 6 is taken over a random seed used to draw a set of finite-width DNN weights and batches of training examples, whereas our model and training procedure are deterministic given a set of metaparameters. Therefore, the expectation in equation 6 is with respect to the choice of metaparameters only.

We include three metaparameters that were not present in (Dziugaite et al., 2020): explicit (diagonal) regularization, training time, and activation function. We omit width, learning rate, and mini-batch size, as these do not apply to our setting. We report the mean and maximum SE over all possible interventions to each metaparameter. For example, for depth, which has a range of 1 to 5, we evaluate the SE arising from changing the depth from 1 to 2, again for 1 to 3, and so on for all ten combinations. Mean and max SE are then evaluated across the ten "before" and "after" configurations. The mean and max SE are identical for the `activation` function which took one of two options: ReLU, Erf. We discard samples with a Hoeffding weight less than 0.5 as per Dziugaite et al. but provide all data in Figure 14c.

Intervening on the amount of `diagonal` regularization and training `time` consistently yields zero mean (Figure 14a) and maximum (Figure 14b) SE. Intervening on the number of `train samples` also yields small mean SE, with the exception of the `0/1` task which had a small mean sample size of only $N = 18$. Two tasks: `0/1` and `3/4` show unusually high max SE for `train samples`, while the rest have small SE (Figure 14b). Therefore, these three metaparameters strongly influence the overall correlation between ICB and GE. Conversely, manipulating the `activation` function and `depth` induced large SEs. Intriguingly ICB, was almost perfectly anti-correlated with GE for interventions to the `depth` with SE ≈ 1.0.

Table 12: Detailed GE prediction SE for all combinations of the `train samples` metaparameter for the CIFAR 8 versus 9 task. The first two columns ("Raw") comprise all SEs with only basic filtering for $I_{\mathrm{UB}}(X;Z) \leq \log(\texttt{train samples})$. The next set of ("Filtered") columns additionally accounts for Monte Carlo variance of empirical averages and discards samples with a small difference in GE relative to the number of train and test samples (see text for details). Sample sizes "N" of under ten are replaced with "–" and omitted from calculations. The final "filtered" mean SE of 13.6% ($N = 28$) appears in Figure 14a, the robust SE of 28.6% ($N = 62$) appears in Figure 14b, and the final "raw" mean SE of 42.2% ($N = 241$) is shown in Figure 14c (series `8/9`).

Raw		Filtered		Metaparameter	
N	Sign-error	N	Sign-error	Low value	High value
239	42.3%	–	–	1000	1250
239	39.3%	10	0.0%	1000	1500
238	39.5%	24	0.0%	1000	1750
239	40.6%	62	22.6%	1000	2000
243	25.1%	–	–	1250	1500
240	35.4%	14	28.6%	1250	1750
243	42.4%	41	19.5%	1250	2000
243	49.0%	–	–	1500	1750
244	57.4%	18	11.1%	1500	2000
243	51.0%	–	–	1750	2000
241	42.2%	28	13.6%	**Mean**	
244	57.4%	62	28.6%	**Maximum**	